DEVELOPING A MULTIFUNCTIONAL THERMO-RESPONSIVE VIRAL LIKE PARTICLE (VLP) PLATFORM WITH NEW PHYSICOCHEMICAL CHARACTERISTICS

SEPEHR DEJDAR

Bachelor of Science in Chemical Engineering

Sharif University of Technology

February 2015

Submitted in partial fulfillment of requirements for the degree

MASTER OF SIENCE IN BIOMEDICAL ENGINEERING

at the

CLEVELAND STATE UNIVERSITY

August 2020

We hereby approve this thesis for

SEPEHR DEJDAR

Candidate for the Master of Science in Biomedical Engineering degree for the

Department of Chemical and Biomedical Engineering

and the CLEVELAND STATE UNIVERSITY'S

College of Graduate Studies by

Thesis Committee Chairperson, Nolan B. Holland, PhD

Department of Chemical and Biomedical Engineering

Date

Thesis Committee Member, Xue-Long Sun

Department of Chemistry

Date

Thesis Committee Member, Christopher Wirth, PhD

Department of Chemical and Biomedical Engineering

Date

Student's Date of Defense: July 31, 2020

ACKNOWLEDGEMENTS

First, I would like to thank my incredible advisor Dr. Nolan Holland, who provided me with the opportunity to work and study in his laboratory. Beside his great mentorship and attitude his patience, insight, intelligence, knowledge, questions, feedbacks, and passion for the science always have been an inspiration and a road-opener during executing my research study.

I appreciate the time my committee members spent guiding me during the process of creating this thesis.

I would like to thank my peers Adil Mistry and Mario Alberto for helping me with trainings and the protocols in the laboratory, as well as keeping science cool during its uncool phase.

Special thanks to Becky Laird and Darlene Montgomery, they always have been there no matter what helping all students and staffs through their affairs and challenges toward their academic goals.

Last but not least my beautiful family whom their unconditional encouragement and support during my entire life always keep my motivation blazing to pursue and achieve “what I have faith in”.

DEVELOPING MULTIFUNCTIONAL THERMO-RESPONSIVE VIRAL LIKE PARTICLE (VLP) PLATFORM WITH NEW PHYSICOCHEMICAL CHARACTERISTICS

SEPEHR DEJDAR

ABSTRACT

Smart materials are a class of material whose physical characteristics change significantly in a controllable fashion once exposed to an external stimulus such as stress, pH, light, temperature, etc. If the temperature is the external stimuli (control variable) the material is termed thermo-responsive. Out of numerous thermo-responsive materials, elastin-like polypeptide (ELP) is a well-known protein-based biopolymer.

Protein cages are well-defined biological nanostructures which are highly symmetrical and monodisperse. This class of proteins are both chemically and genetically tunable, making them a suitable recipient of new properties. Protein re-engineering is the basis of developing a hybrid platform (e.g. polymer-protein) to deliver some new functionalities and tasks. Prolonged delivery, sustained drug loading/ release, and targeting delivery are the challenges that led to introducing novel biohybrid materials to tackle shortcomings of existing drug delivery systems. Among all possible structures, a thermo-responsive VLP (viral like particle) was designed for a potential ultimate application in drug delivery. In the designed structure the outermost shell of the bacteriophage P22 (in its empty shell form) is homogenously decorated with ELP as each coat-protein subunit (CP) is genetically fused with a fusion tag polymer (ELP). Those recombinant subunits (CP-ELP) are self-assembled through intermolecular interactions (non-covalent bonds including hydrogen bonds, electrostatic bonds, etc.) in a highly repetitive array to end in a hairy-ball structure.

The art of gene design was incorporated with synthetic biology techniques to accomplish the idea behind this research. Utilizing these tools, a versatile genetic code with appropriate cut-sites to be edible at the C-terminus of coat protein (CP) for adding pentapeptides with different lengths (or any other peptide sequences with appropriate overlaps) was designed. After synthesizing the ELP-fused particle with different lengths, characterization assays such as dynamic light scattering (DLS) and UV-VIS spectroscopy were conducted to investigate the thermal-behavior of synthesized particles. These data along with scanning electron microscopy (SEM) confirm the formation of hybrid particles with predicted morphology.

This work clearly has demonstrated the feasibility of a recombinant self-assembled nanocage structure modified with thermally responsive peptides. Such structure could comprise some potential applications in the biopharmaceutical industry and more specifically drug delivery systems.

TABLE OF CONTENTS

PAGE

LIST OF TABLES

TABLE PAGE

LIST OF FIGURES

FIGURE PAGE

CHAPTER I

INTRODUCTION

Nanotechnology refers to a highly interdisciplinary field connecting fields of study such as physics, material science chemistry, biology, medicine etc. The fact that a majority of biological processes occur at the nano-scale level, gives scientists an opportunity to tangibly control chemical processes and interactions on the molecular level. Recently a wide range of biological molecules and materials have been exploited within the nanotechnology industry and more in particular nanomedicine. Biological nanomaterials, namely nucleic acids and proteins could be utilized as remarkably promising platforms for pharmaceutical applications (1, 20).

Out of those platforms, viruses have emerged as an elegant platform in nanotechnology for synthetic manipulation with a various range of applications from medicine to making batteries. Viruses are classified as the non-living class of materials as they are unable to live and reproduce outside of the host cell. The essential common nature of all viruses is to infect a host cell and replicate, packaging its nucleic acid using the cell's machinery and ultimately exiting the cell. Viruses are the most abundant biological entity on the planet

(some sources debating on at least 10^{31} inhabitants in the biosphere) and second in terms of biomass after prokaryotes (4, 5). That diversity could be exciting for researchers and virologists on one side and it might be challenging to exploit such diverse systems due to numerous options on the flip side. Incorporating new functionality in protein cages is feasible by chemical and/ or genetic manipulation. Also, those manipulations could uniquely be applied to the whole structure since the architecture of viruses is nothing but assembly of repeating subunits which form highly symmetrical, multivalent, and homogeneous structure (2, 3).

Another essential protein construct, that has been utilized within the context of this thesis, is elastin-like polypeptide (ELP). ELPs refer to a group of peptide-based and stimuli-responsive materials that go through phase transition in response to an external stimulus. In the case of ELPs, the stimulus can be temperature, pH, or other solution properties. ELPs are soluble below their lower critical solution temperature (LCST) and phase separate forming a coacervate above their phase transition temperature (6, 7). The ELP that is utilized for this study has the sequence of $(\mathrm{GVGVP})_{\mathrm{n}}$, in which n is the number of pentapeptide repetition.

The primary purpose of this study was to synthesize a stimuli-responsive viral like particles by recombining two proteins of interest i) viral like particle (VLP) coat protein and ii) ELP. The array of 420 pentapeptides on the surface of each particle is expected to form an ELP-dense outer layer. Such a hairy spherical structure could be utilized as a multifunctional platform, which the cumulative effect of pentapeptide arms gives the particles a new functionality of thermo-responsive behavior.

1.1. Viral Like Particles (VLPs) and Their Potential Applications in Biotechnology

The main functions of the cage, or capsid, of a virus is to protect the viral genome, and facilitate the infection process. Most of viral capsids are composed of protein subunits (in some cases are surrounded by a phospholipid bilayer); hence the three-dimensional structure of these viral capsids is a function of the protein geometry and protein-protein interactions. These nanostructures are mostly self-assembled spherical hollow-shape particles (derived from viruses or other biological resources) with 22-390 nm in diameter (1, 8).

Viral cages which are assembled without nucleic acid are called virus-like particles (VLPs). These VLPs most often maintain the symmetry of their viral source of origin while do not have the potential of the viral source to infect the host cell and propagate (1, 20).

VLPs are simple and elegant systems that exist in both living organisms and non-living biological systems (9). Furthermore, their surface characteristics and versatility in mo difications make them programmable and tunable candidate to be functionalized over a broad range of molecules for numerous applications (1). Diverse applications such as vaccine development, enzymatic carbon fixation of carboxysomes, the generation of vitamin B2 by the capsid forming enzyme (lumazine synthase), nanoreactors for encapsulation of catalytic reactants or active enzymes, and iron storage of ferritins are robust examples of these types of nanocages (10, 11)

With growth acceleration in the number of viruses (including both wild-types and engineered ones); researchers are projecting that the diversity in this type of system will surpass any other genetically replicable biological system (12).

1.2. The Structure of Virus Capsid

Different viruses may adopt one of a remarkably diverse range of structures that can be divided into four main groups of icosahedral, rod-shaped: either helical tubes or filaments, Enveloped , and Complex (1)

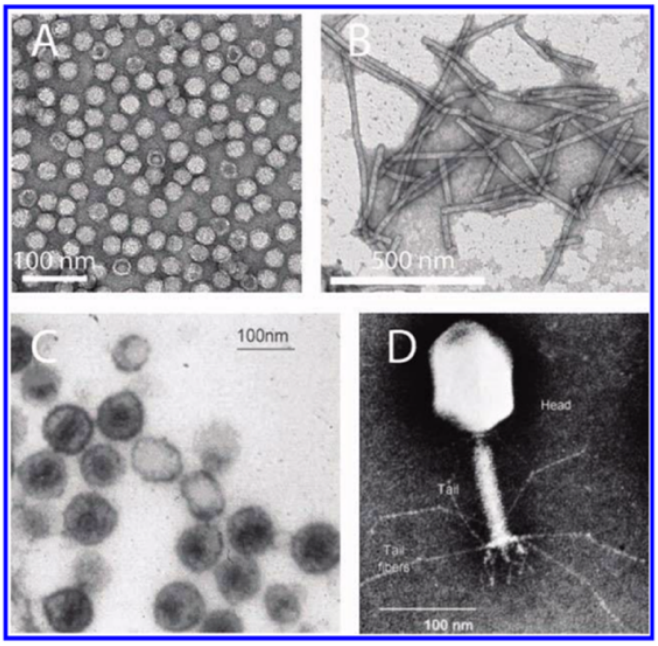

Figure 1. Different virus structures are illustrated using transmission electron micrographs. A) "Cowpea mosaic virus" represents an example of icosahedral particle B) "Tobacco mosaic virus" represents an example of rod-shaped particle C) "Human immunodeficiency virus 1" represents an example of enveloped virus D) "Bacteriophage T4" represents an example of head and tail complex virus structure (1)

Twenty different case studies of VLP platform are currently being utilized in different nanotechnology area applications, in which 13 are non-enveloped with icosahedral symmetry, 4 are non-enveloped rod-shaped, and 3 are enveloped (13, 14). Icosahedral particles have garnered more attention than other structures due to their abundance, stability, and biocompatibility. Therefore this study addresses only this specific type of viruses.

Icosahedral symmetry stems from the word icosahedron, which in Greek means "twenty seats": an icosahedron is a polyhedron with twenty faces, and it is the largest closed configuration that is constituted of identical units (the coat protein). For instance, an icosahedral particle made up of 60 coat protein subunits is arranged in a way that 3 coat proteins are placed on each triangular faces in an equivalent manner.

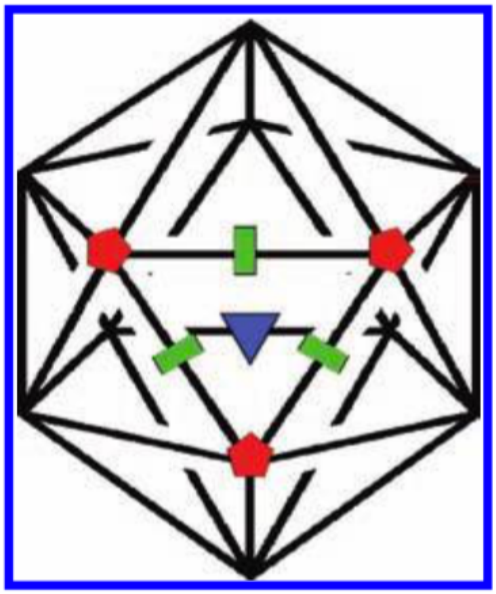

Figure 2. This is an illustration of an icosahedron including 20 triangular faces and the symmetry of 5:3:2. Red pentagrams show fivefold axis, blue triangles show threefold axis, and green rectangles show twofold axis (1)

Quasi-equivalent symmetry is defined for larger structures that are formed by more than 60 subunits. In such symmetry, subunits cannot be placed at equivalent positions. The geometric principles of this theory were developed by Caspar and Klug in 1962, when they proposed the triangulation number (4). Following their theory, the virus capsid in icosahedral conformation consists of both pentamers and hexamers. A virus capsid in different ways is alike soccer ball constituted of pentagons and hexagons, in which bonding orientations are not identical. This distortion is so-called "quasi-equivalence." In this structure pentamers are inserted in exchange for some hexamers at certain points, according

to some geometry base on the T number. The relative position of the hexamers can be indexed along the axis denoted by h and k, which are related by a 60° rotation. The mathematical relation obeys the following formula:

$$T = h^2+hk+k^2$$

Where h and k could take any positive integer or zero and consequently T numbers can only be positive integer values. The size of capsid is proportional to the T number; the higher the T number the larger size the capsid could attain (1, 15).

Generalizing the concept would help to derive more relatable equations between T number, number of pentamers, and hexamers:

#Pentamers: 12 (always constant, regardless of T number)

#hexamers: 10 x (T-1)

#Protein subunits: 60 x T

In general, minimum-energy capsid structures corresponds to those with the minimum number (T=1,3,4,7, …) of inequivalent positions for 60 x T protein subunits (1).

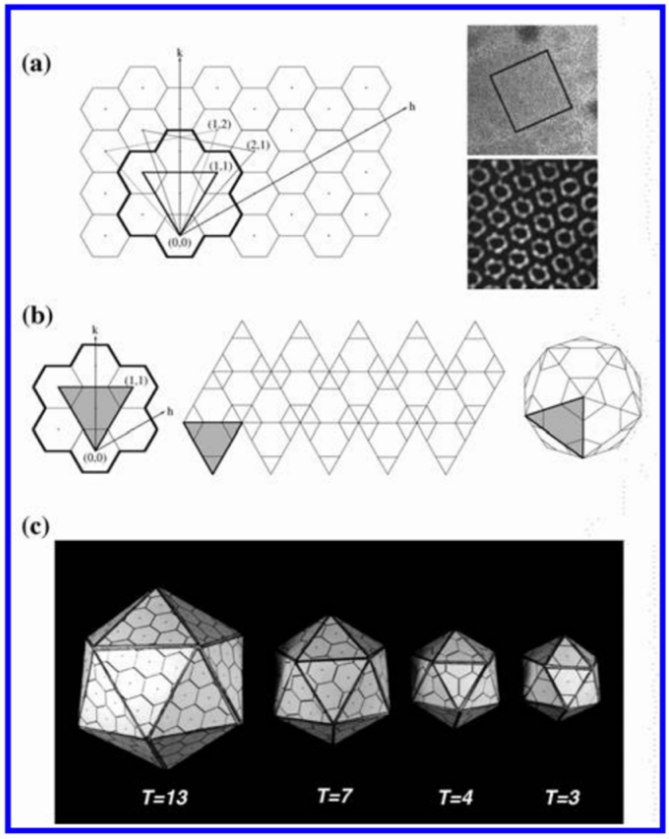

Figure 3. The geometric principles for generation of icosahedral quasi-equivalent structure of a lattice. a) The initiation of the construct creation is with the planar hexamers, while adding pentamers will introduce curvature (they go and sit on each vertex). The closed-structure is not viable unless 12 pentamers are inserted at appropriate positions in the hexamer net. The positioning of these pentamers is assigned by (h, k) coordinate as it is shown in the figure. In this system, the origin also is replaced by a pentamer. b) A three-dimensional model of lattice folded to make a quasi-equivalent icosahedral structure with T=3 (h=1, k=1). c) Cardboard models of several icosahedral quasi-equivalent surface lattices with a different T number (1)

1.3. Genetic Versus Chemical Modification of Protein Cages

To enhance a unique characteristic for a particular application, one may modify the protein cage platform either genetically or chemically. Chemical modification potentially suffers from some significant drawbacks such as being time consuming and a multi-step process, as well as consisting of non-specific chemical labeling steps. On the other hand, genetic labeling is a stoichiometrically-controlled and robust method for the multivalent, isometric, homogeneous, and site-specific labeling approach (1, 72). However, at the same

time genetic modifications are often limited by the structure of the protein cages, and specifically must be adapted for each individual platform. One of the big challenges that researchers encounter as they incorporate genetic fusion is to maintain the original structure of the platform without any disruption. A single point mutation in the subunit of a protein cage can result in failure of assembly thoroughly or converting of the assembly into an alternate morphology (16, 17). As an example, fusion of cysteines on the CPMV exterior capsid leads to disulfide bond formation and as a result, capsid aggregation (18). All of genetic or chemical modifications could be applied on three available amenable sites: interior, subunit interface, and exterior of the cage architecture (19, 20).

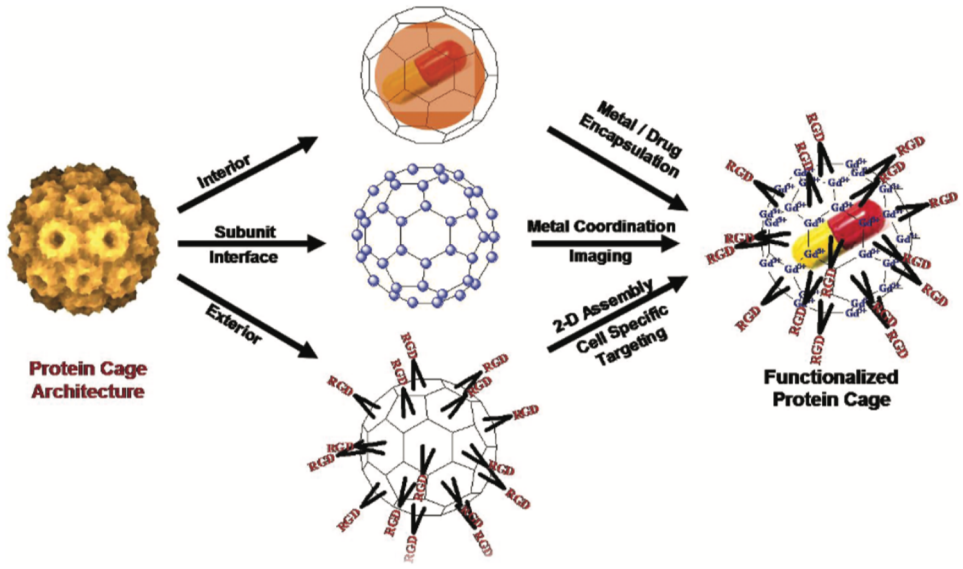

Figure 4. Possible types of surface modification and their applications (20)

1.4. P22 Bacteriophage

Bacteriophage P22, which infects Salmonella enterica serovar typhimurium, is a tailed dsDNA bacteriophage and has the potential to assemble into a procapsid. This nano-construct is constituted of 420 copies of 46.6 kDa coat-protein (CP) subunits, maintaining

an icosahedral (T=7) geometry with the final diameter of 58 nm. The assembly process could be catalyzed in a more organized morphology by assisting 60-300 copies of 33.6 kDa Scaffolding Protein (SP) (21, 22).

Ionic interaction between scaffolding and coat protein is counted as the major driving force for assembly of P22 procapsid (23). The binding domain within the scaffold protein construct in charge of scaffold-coat association is a helix turn helix structure near the C-terminus with highly charged surface. While the C-terminus of SP interacts with CP, the N-terminus can be severely truncated or mutated with little to no effect on assembly (23-25). The presence of scaffolding protein results in proper, organized, and quasi-symmetry (T=7) assembly of coat protein subunits to form a procapsid (16).

P22 maturation is driven by tuning the weak quaternary subunits interaction with a final mature expanded capsid (T=7) quasi-equivalent symmetry. This transformation provides mature P22 with a relative rigid assembly with a stabilized hydrophobic protein core and ehnhaned hydrogen bonding network. There are two stages assembly in P22 maturation. In the first step, identical coat subunits form a weaker structure (procapsid). In the second step, capsid expansion results in a mature and stable quasi-equivalence structure. Such biophysical transformations has a great imapct on the stability of protein structures under external stresses such as heat and protein denaturants (26).

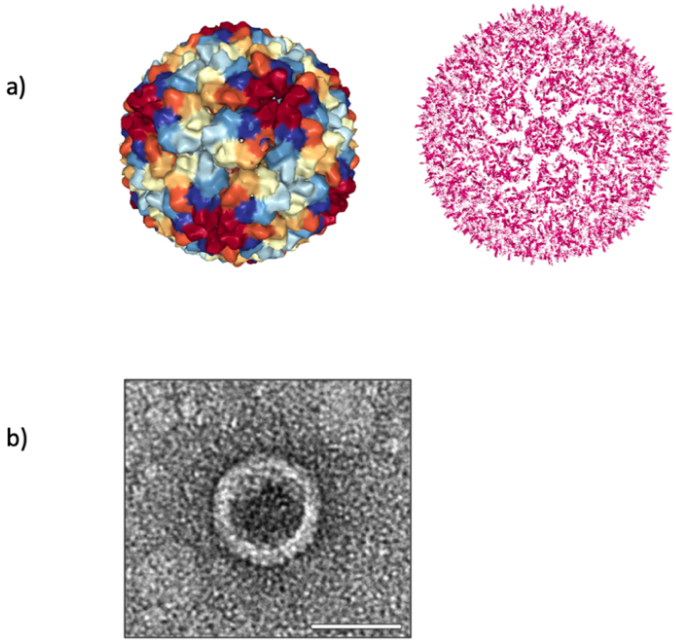

Figure 5.a) cryo-EM reconstruction of the P22 VLP (PDB: 2XYY) shows a T=7 icosahedron (60 hexamers, 12 pentamers) approximately 58 nm in diameter b) TEM showing the P22 VLP, Scale bar is 50 nm (27)

1.5. Non-Infectious P22 Capsid and Its Various Morphologies

To generate non-infectious P22 capsid, two proteins (scaffold and coat) are sufficient. Mixing in vitro or co-expression of two proteins within E. coli leads into the formation of isomeric procapsid in which in this conformation, portal protein is substituted by 5 additional copies of the coat protein (30).

The capsid morphology will change with temperature and chemical treatment (Figure 6). Four different morphologies have been reported: i) Procapsid (PC) ii) Empty Shell (ES) iii) Expanded Shell (EX), and iv) Wiffle Ball (WB). Incubation of PC with 0.5 M guanidine hydrochloride (GdmHCl) produces an empty shell (ES) by releasing the scaffold proteins (28). Heating up to 65°C for 20 minutes irreversibly expands the capsid and alter the conformation to an expanded shell (EX) with a diameter of 64 nm (29). Heating of ES at 75°C for 20 minutes leads to release of pentons from fivefold axes (vertices in an

icosahedral structure) and leaves 10nm pores to produce the wiffle ball (WB) conformation. Some of the conformations mimic the transient structures during capsid maturation and DNA packaging, for instance "expanded shell" mimics the structure of the virus head filled with DNA (30).

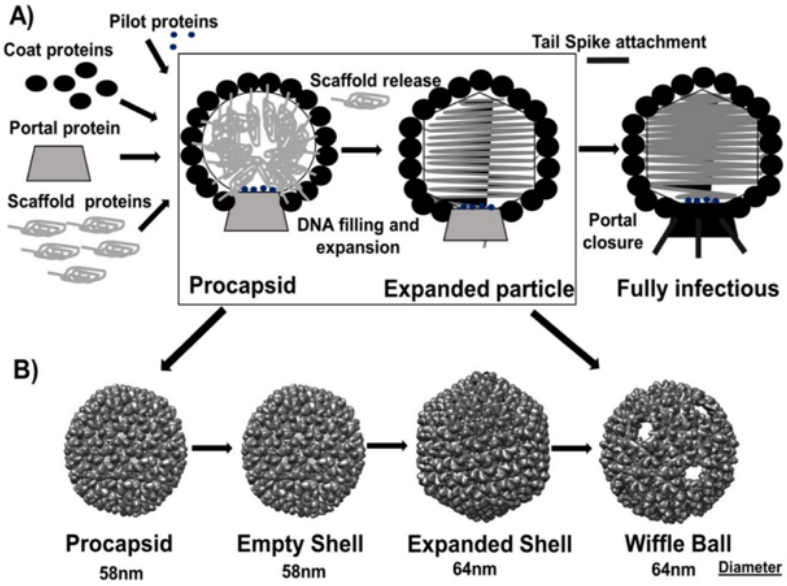

Figure 6. P22 capsid maturation and its intermediates. A) In vivo assembly for infectious P22 B) different intermediates of P22. Procapsid is composed of both scaffold and coat proteins, while empty shell is only made up of coat proteins. Expanded shell is the enlarged icosahedral version of empty shell while wiffle ball is missing pentamers (on the vertices) of the expanded shell configuration (30). (PDB ID: Procapsid-3IYI, Expanded Shell-2XYZ, Wiffle Ball-3IYH)

1.6. P22 Structure and Stability in the Absence of SP

There are a few potential functions of scaffolding proteins including DNA packaging, size regulation, exclusion of cellular proteins from the assembling capsid, and so on (31, 32). By proposing several models, the scaffolding proteins are directly involved in conducting the interactions of the coat proteins (with different quasi-equivalent) conformations, resulting in the formation of appropriately-sized (T=7) P22 procapsid (33).

However, it has also been shown that P22 capsid stabilization stems from the interactions of N-terminal helices and an extensive "P-loop." That bonding is robust enough that it eliminates any need for cross-links or auxiliary proteins. The indicative structural studies using cryo-electron microscopy (cryo-EM) demonstrate that, in the absence of scaffolding, coat proteins form both wild-type sized and smaller sized capsids, T=7 and T=4, as well as aberrant spiral structures; however, with lower fidelity. It is noteworthy to know that a P22 coat protein is made up of two different domains (Figure 7) according to the existing models (22, 34).

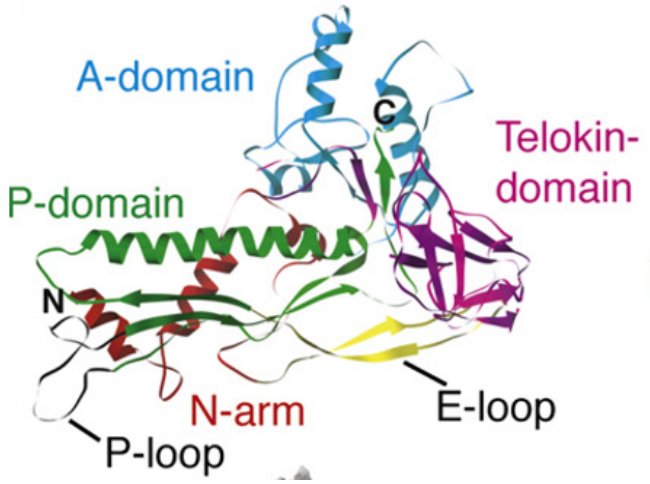

Figure 7. P22 subunit structure and residues location (22). The color-coded domains are: N-arm (Red), E-loop (yellow), P-domain (green), A-domain (cyan), telokin domain (magenta)

1.7. P22 Exterior Surface Modification

Even though research indicates possibilities for P22 surface modification, those modifications have shortage of options for the exterior surface modification (interior modification is the focus of most of those studies) (25, 30, 73). Some of the research demonstrates the C-terminus fusion of CP including the adhesion of motifs, tags and short peptides. The intact expression, folding, and assembly of these genetically-modified constructs could be addressed by some examples: fusion of histidine tag (6XHIS), -K-Coil,

and -E-Coil to the outermost of the P22 shell (36, 37). Also under a series of genetic mutations and biochemical characterizations following up the utilization of the cryo-EM technique, researchers discovered that C-terminus of coat protein (CP) extends toward the capsid exterior (17, 38, 39).

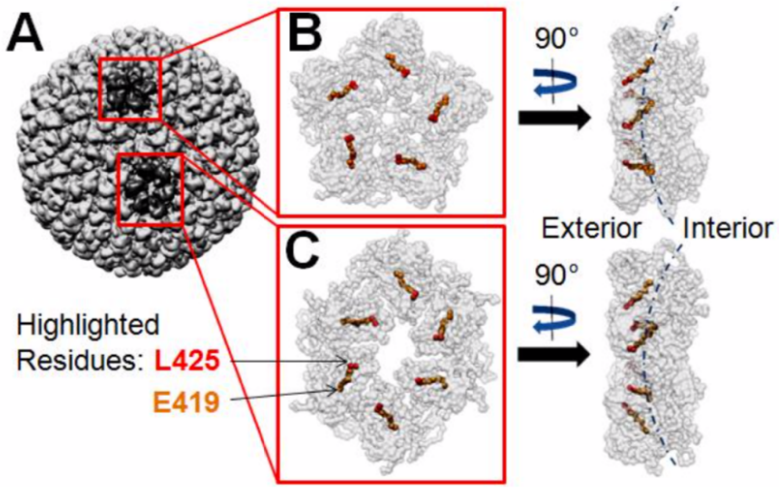

Figure 8. A) a representation of P22 procapsid from the published Cryo-EM structure, which includes residues 1-425 of the 430 amino acids of CP. Residues 419-425 (the last 5 amino acids are not resolved and their location is ambiguous) are highlighted in the zoomed depiction of the B) Pentamer and C) Hexamer Units, which in both of the CP C-terminus extends towards the capsid exterior (Reprinted with permission from (36) Copyright (2013) American Chemical Society)

1.8. Elastin-Like Polypeptides and LCST Behavior

Elastin like Polypeptides (ELPs) refer to a repeating sequence of poly-(VPGVG) found in elastin (a natural protein which formed the embodiment of extracellular matrix) within the broad range of chain length that are both temperature responsive and biocompatible. ELPs exhibit lower critical solution temperature (LCST) behavior, such that they are soluble in aqueous solutions below their phase transition temperature (T_t) and undergo a phase transition if the temperature rises above T_t which results in desolvation and aggregation of the polypeptide. This aggregation process is reversible upon cooling below

T_t. Since, ELPs consist of natural amino acids, they are potentially more biodegradable and biocompatible than polymers composed of synthetic building blocks (44, 45).

These characteristics raise the interest of utilizing ELPs as a smart material for various applications in nanomedicine. There are several studies that address the transferring of LCST properties from ELP onto a molecule fused to it (including small hydrophobic drugs, protein receptors, ssDNA, and virus coat proteins) (46, 47). In another study, the enhanced permeability and retention (EPR) of these ELP nanoparticles for tumor targeting have been reported (48).

1.9. ELP-Based Nanoparticle Systems

Out of numerous advantages of ELPs, here the applications of this biocompatible, tunable, and smart material in the areas of particle formulation and surface modification is elaborated. Those characteristics make ELP a useful component in the drug delivery system, in addition to conferring their stimuli-response behavior to other materials. Both fully developed ELP-based and ELP-hybrid materials (reported by different literatures) are discussed here.

1.9.1. ELP Di-Block Copolymer Micelles

ELP-based nanoparticle formation in a stimulus-responsive manner is difficult without an appropriate design of this biopolymer. In a tunable manner one could develop a di-block copolymer that relies on at least one ELP block to mimic their thermo-responsive behavior. However, the other block could be either an ELP sequence or any other molecular chain. Figure 9 is a demonstration of Hydrophilic-ELP and Hydrophobic-ELP di-block copolymer. These monomers are designed so that each block has a significant difference in T_t compared to one another. Since the hydrophobic part has a lower T_t than the

hydrophilic part, there is a range in which the hydrophobic block is in its condensed conformation while the hydrophilic block is in its own random coil structure (between CMT and $T_{aggregation}$). The ignition of micelle-like structure formations is due to ELP blocks amphiphilic characteristics within a temperature range. Heating over the hydrophilic block transition temperature (T_t) results in the collapse of micelle morphology (49, 50).

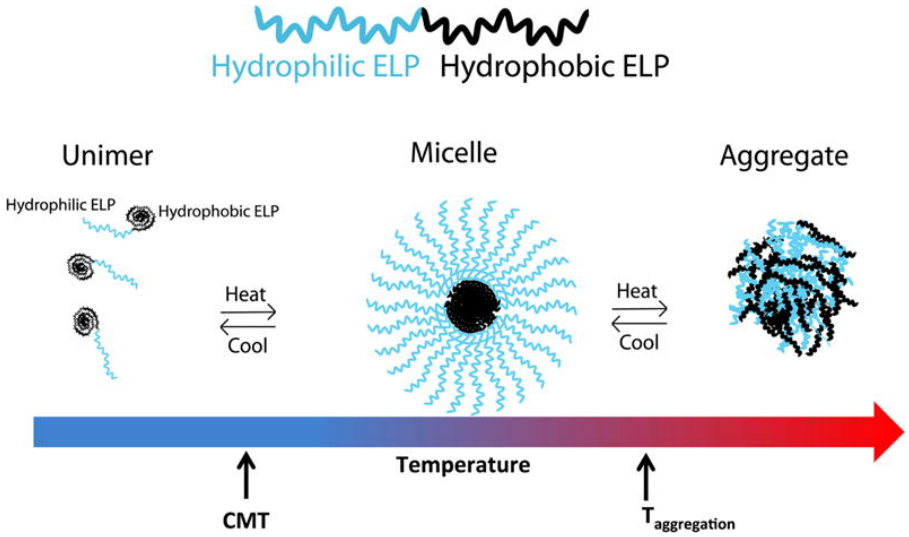

Figure 9. Self-assembly of ELP di-block copolymer. Below the critical micelle temperature (CMT), monomers are soluble. Increasing the temperature above the CMT, the hydrophobic core starts to form while hydrophilic blocks, in their own natural coil structure, form the corona of the micelles. Upon heating up to above $T_{aggregation}$, the hydrophilic part also turns into an insoluble fraction, and the micelle structure starts to collapse (76)

1.9.2. Hybrid ELP Systems

ELPs are able to confer their stimuli-responsive behavior to the other materials, which are also are well-known as the class of "ELP-functionalized platforms." A generation of hybrid liposome-ELP nanoparticles with rapid self-assembly characteristics in response to the temperature gradient with high-dosage/ slow release encapsulation capability of DTX (as drug compound) is a practical example for such functionalized platforms (48). ELP-

modified liposomes presented an enhanced cellular uptake versus no ELP attached liposomes. The gastrin-releasing peptide receptor (GRPR) is overexpressed in prostate cancer cells. In this study, a gastrin releasing peptide (GRP) is appended to the ELP-nanoparticle's surface for a targeted delivery (48).

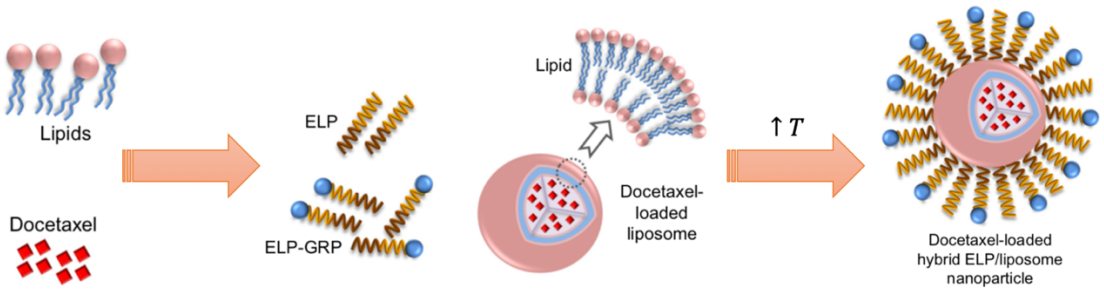

Figure 10. Hybrid ELP-nanoparticles with targeting capability of prostate cancer cells. At the first step, DTX is encapsulated with the liposomal nanoparticles. In the second step, mixing the particles and recombinant ELPs following up the raising of the temperature results in self-assembly of hybrid nanoparticles (Reprinted with permission from (48) Copyright (2018) Dove Medical Press.)

In another individual study, ELP-trimer attached to a foldon (hydrophilic head group) was shown to form foldon-micelles. By increasing the temperature over the transition temperature of hydrophobic chains, the ELP chains are arrayed within the core of micelle while the foldon domains are situated on the exterior, and as the corona of the micelle (49-52).

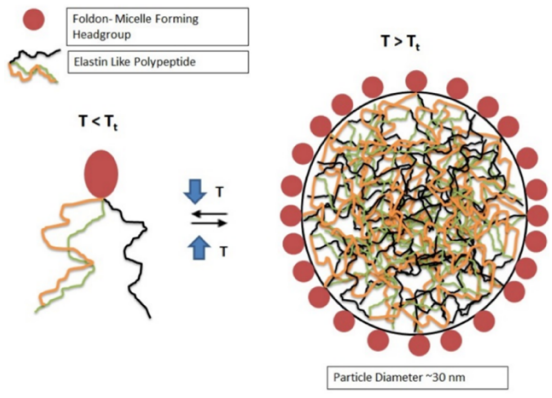

Figure 11.ELP-foldon micelle formation schematic (52)

One other studied hybrid system is ELP-functionalized plasmonic nanoparticles. More specifically, ELP-functionalized gold nanoparticles were fabricated through ELP adsorption onto mercaptoundecanoic acid (MUA)-modified spherical gold nanoparticles (53). The thermal-response behavior of ELPs was conferred to these hybrid particles such that an increase in the system's temperature ends up in reversible aggregation of the gold nanoparticles within the solution above the ELP transition temperature. Another way is to covalently attach ELPs onto a GNP surface by coupling an amine group on the ELP's N-terminus, which will result in MUA surface activation. However, aggregation achieved with covalently grafted ELPs is less likely to be reversible than the aggregation achieved with adsorbed ELPs (54).

1.10. Motivation to Design a Synthetic Hybrid VLP Platform

The emergence of recombinant DNA technology has greatly enhanced the possibility of creating almost any desired recombinant protein (with a precise and predefined sequence), even to a larger extent than what conventional nature or any chemistry can achieve. Thanks to synthetic biology, one could controllably modify the design of, and/ or tune these recombinant DNAs toward making a whole new protein structure that contains specific physicochemical characteristics (that might never exist in the nature or elsewhere). A common way to produce these recombinant proteins is to use bacteria as a protein-production factory. Bacterial transformation refers to the transformation of the plasmid encoding the protein of interest. This plasmid-construct is commonly generated by the digestion/ assembly method prior to the transformation.

Out of numerous possibilities for the recombinant protein production, recombinant expression and isolation of an ELP-tagged VLP with completely novel characteristics

could potentially open many doors toward introducing a new class of biohybrid materials, which could have interesting applications. This multi-facet platform exhibits the responsive nature of the ELP while retaining the multivalent structure of the protein cage.

We envision that a hybrid protein-biopolymer vesicle could be a promising candidate for medical and material applications because of its mono-dispersity and bioactivity. A prominent application of this stimulus-responsive platform could be sustained drug loading/ release to tumor cells using in vivo localized heating techniques (e.g. medical device, exciting magnetic particles, etc.). The temperature-dependent concentration of these nanoparticles could potentially could enhance the permeation and retention of such nanocontainers, especially at a mild, clinical-hyperthermia state- which is 42°C (e.g. the high concentration of nanoparticles sticks around tumor tissue). Moreover, altered surface chemistry in such particles (with added pentapeptides on the particle's surface) could greatly help with evading the immune system's response and, as a result, the prolonged circulation time within the body.

It is also possible to enhance the cellular uptake of nanoparticles by appending a cell-penetrating peptide (CPP) to the one free end (C-terminus) of the ELP; however, that is out of the scope of this project.

In the realm of protein engineering (and also this study), the challenge of such manipulations is to create a new and meaningful structure (and not a gibberish structure) that has desirable functionalities. However, this principle is not attainable without contemplating the pathway of the design. The challenge in this study is making a hybrid ELP-protein of CP-$(VPGVG)_X$ (in which the X is the number of repetition), yielding a library of CP with an ELP-tags attached to it (ELP chain length is changeable in this

library). In such systems, the constructs are capable of self-assembling into particles under standard physical conditions. In this study, we confined the protein engineering to C-terminus modification of CP, with four different lengths of polypeptide (X=1, 10, 20, 40).

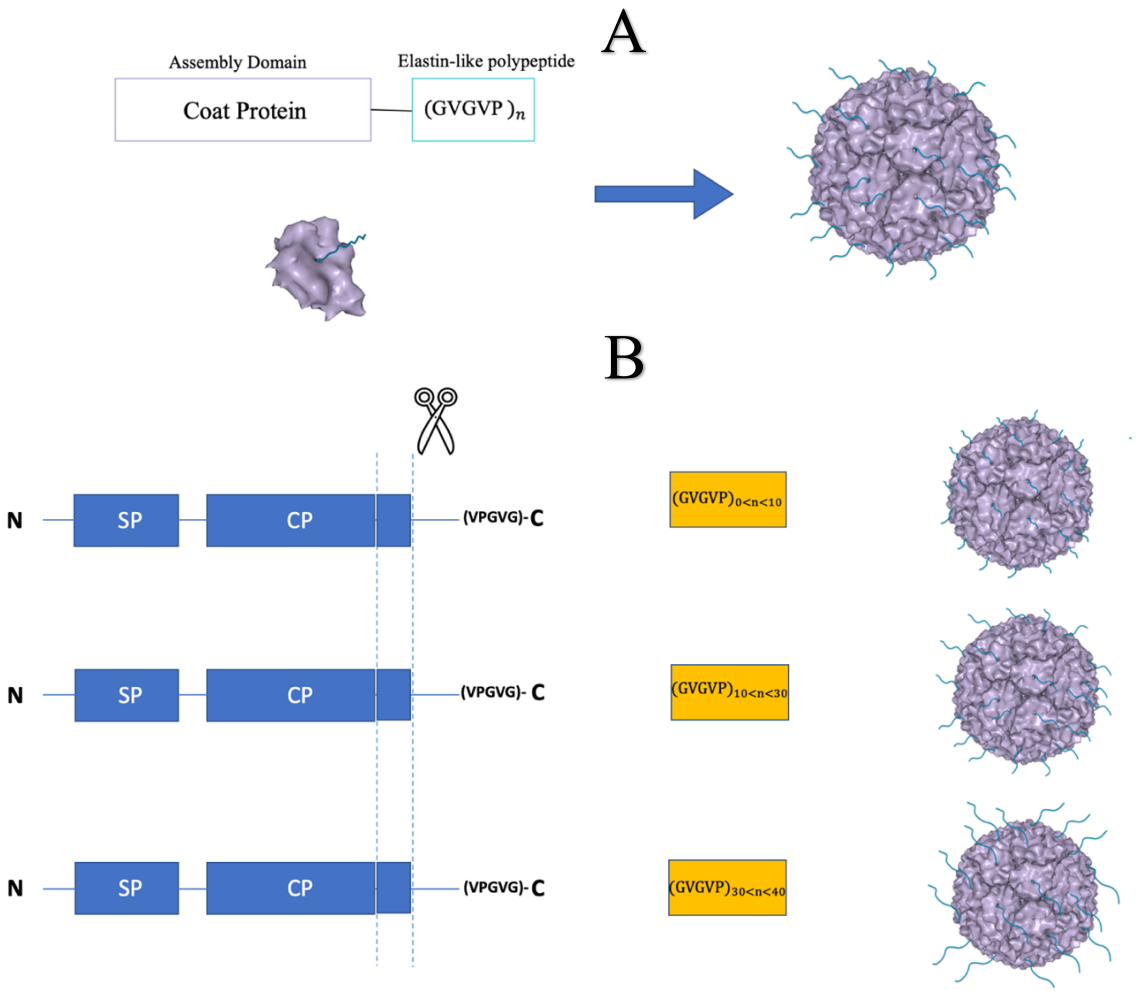

Figure 12. A) ELP sequence (GVGVP)n downstream of the assembly-domain (CP) will arm each assembly-domain with a fusion tag. Finally, 420 of these subunits start to assemble into a nanoparticle structure B) P22 C-terminus modification with different ELPs chain length. The dotted region could be substituted with desired ELPs (yellow boxes).

CHAPTER II

MATERIALS AND METHODS

2.1. Genetic Design

2.1.1. Preface

The biotechnology field of study started to flourish with the emergence of DNA-exploration, and the decoding of its genetic construct. Who would have thought, a half century after that discovery, that human beings would be able to design and create any recombinant DNA? Thanks to genetic engineering, scientists can read, write, and edit the DNA. Nowadays various corporations can compose the desired DNA-sequence in a matter of days. The ability for those companies to make DNA sequences might sometimes be limited, or the DNA sequences are unable to be expanded, yet we could tune our needs to their potentials. Having a long, complex DNA-sequence for the wild-type structure of P22 further increased the time and fees required by the manufacturing company.

2.1.2. Design a Versatile Plasmid System

The system that we are trying to design is counted as a multi-protein complex system because it contains two transcription units, each responsible for one protein. The complex term stands for high affinity, protein-protein interaction. Traditionally, such systems used to be expressed in vitro, which meant that each protein had to be expressed and purified individually (in the absence of each other) (57). For a few years, researchers were looking to find a better alternative in order to prevent some of the drawbacks of in vitro expression methodology, such as low-level protein production, protein aggregation, extra steps for purification, and difficulties in the refolding of proteins. Co-expression is a promising alternative approach in which different gene subunits are presented within the context of one vector for simultaneous gene expression (55-57).

The main-vector is designed for the co-expression of two target open reading frames (ORFs), as there are two different coding sequences of scaffolding and coat proteins (SP and CP). Those genes are converted into protein molecules by means of the transcription (DNA to mRNA) and translation (mRNA to protein) processes. The main vector architecture which is inspired by other studies (36, 37) (originally pRSFDuet-1 Vector) contains two multiple cloning sites (MCSs), each of which is preceded by a T7lac promoter and ribosome binding site (RBS). Also, due to the existence of the T7 terminator in the context of pET20b, the T7 terminator sequence is not added into the vector. Noting that, the final cloned version of SP_CP in pET20b has a unique T7 terminator downstream of SP belonging to pET20b.

Referring back to what was discussed in the earlier chapter (**section 1.7.**), we designed a platform in which the ending part (C-terminus) of CP would be modifiable with a

different length of pentapeptide chains $(GVGVP)_X$. It is also noteworthy to recall that the C-terminus of SP interacts with the CP during the self-assembly while N-terminus could be truncated with little or no effect on assembly (25, 58). Hence, it is typical to severely truncate the first 141 amino acids (leaves 162 amino acids) encoding for SP, called SP_{141}.

The genetic codes for both scaffold and coat proteins are taken from the protein data bank (PDB). 2gp8 and 2xyy represent the PDB IDs for both SP_{141} and CP_Wt (wild-type coat protein). Different restriction endonuclease recognition cut sites were incorporated in the designed plasmid. Such a design enables the plasmid to be versatile for further modifications and will be addressed more in detail by the next section.

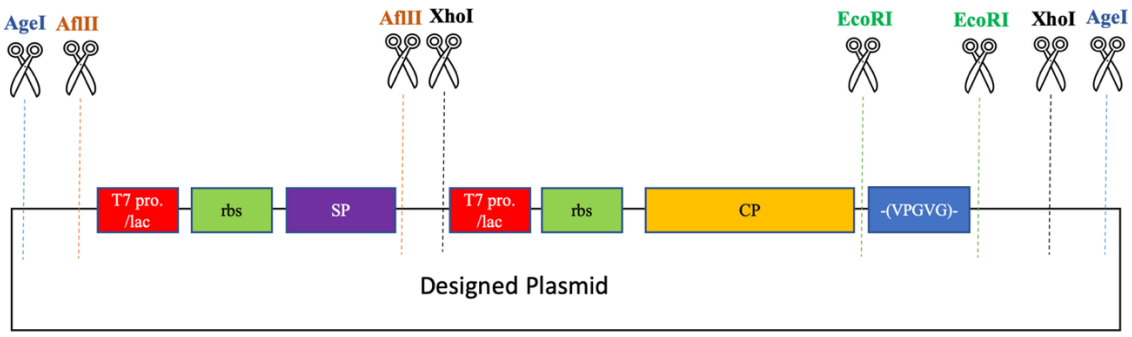

Figure 13. A representation of the designed plasmid with its essential elements

The design of the plasmid (Figure 13) facilitates the generation of two proteins with the ability to add interchangeable fusion tags at the C-terminus of CP. In this case, the interchangeable fusion tags are repetitive pentapeptides, $(GVGVP)_X$, which could be substituted with a -(VPGVG)- sequence within the original plasmid. This pentapeptide sequence (VPGVG) is objectively being placed in the design for further study.

Meyer and Chilkoti, demonstrated that ELP pentapeptides can be synthesized using a recursive directional ligation method (43). Previously, these constructs with various chain lengths were synthesized in our research group (63, 70). We utilized three available ELP

lengths of $(GVGVP)_X$: X=10, 20, 40. The final assembler plasmid is displayed in Figure 14.

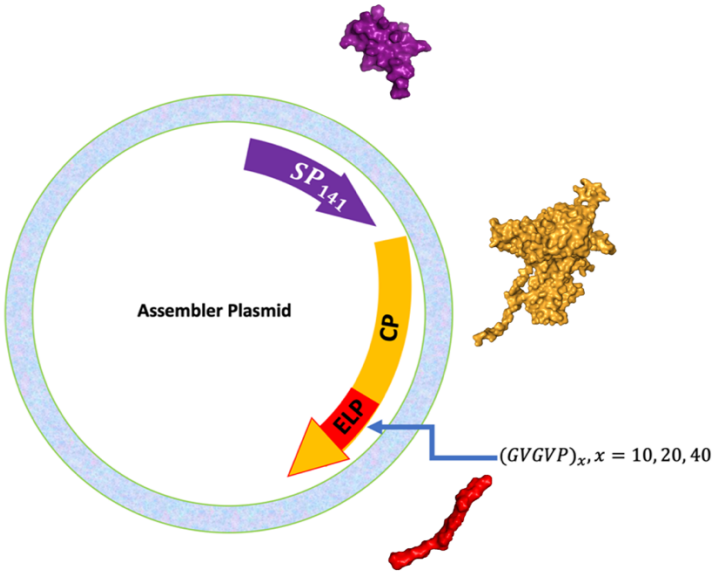

Figure 14. Assembler plasmid for harvesting the protein of interest. This plasmid is attained after executing some experimental molecular biology steps

2.1.3. Genetic Design in Detail

What was described above was the general outline of the genetic design. In this section, the step by step process of designing the final designed gene is described. The arrangement of each restriction site and its downstream and upstream genome sequences are incorporated into the final version of gene-construct such that enables us to not only clone the gene into pET20b, but also to eliminate each gene (SP or CP) in case of necessity. Besides the switchable site for adding ELPs with different lengths or any other different tags with appropriate Gibson overlaps adds extra flexibility for purposeful future modifications. These are two important objectives of the design.

The starting point is to evaluate the options for selection of the recognition cut sites that need to be incorporated within the context of the gene, sticking to the fact that all cut

sites should be unique at that specific site (and not anywhere else in the gene context). For instance, if the plan is to use BSaI for Golden Gate, we must first make sure that the final plasmid lacks that cut site anywhere else in its sequence to avoid inadvertent and undesirable cuts in the gene. The fact that some unique cut sites are situated in the pET20b cloning region can be considered as the starting point for the design. It was decided to totally eliminate the entire cloning region of the pET20b vector, starting at BglII cut site to XhoI cut site during the first digestion reaction. There are two main reasons for doing so: i) the gene was designed with the T7 promoter, which makes it self-sufficient with no needs to the original pET20b T7 promoter, and ii) with that cloning site elimination one could get more options for the restriction site selection (Typical cut sites such as AgeI, EcoRI, NdeI, etc. exist within the cloning site). The eliminated region (cut with BglII and XhoI) is the place where the SP_CP gene would be inserted.

On either extreme of the designed SP_CP, two identical recognition cut sites of AgeI are incorporated, which is recognized as the sequence of ACCGGT. By cutting the desired gene with AgeI, one may clone the gene (with appropriate overlaps) into pET20b cut with BglII and XhoI. To add those overlaps on the 5'-end and right after this AgeI cut site (toward 3'- end), Gibson homology that contains 15-25 nucleotides and is compatible with pET20b sticky overhang on the BglII cut site was incorporated. On the 3'-end also another overlap was incorporated, but this time it is compatible with the pET20b sticky overhang on the XhoI cut site. The digested SP_CP (with AgeI) is chewed back by exonuclease (5' to 3' direction) and leaves a T nucleotide on 5' overhang. To add a corresponding Gibson homology, a frame of 23 nucleotides on pET20b, which ends up with "T" was selected. Similarly, for the 3' overhang, the final Gibson homology of 17 nucleotides ending with

"A" was selected. This process (digestion/ assembly) on the 5'-end is shown in terms of sequences, for a better understanding. The underlines stand for Gibson homology:

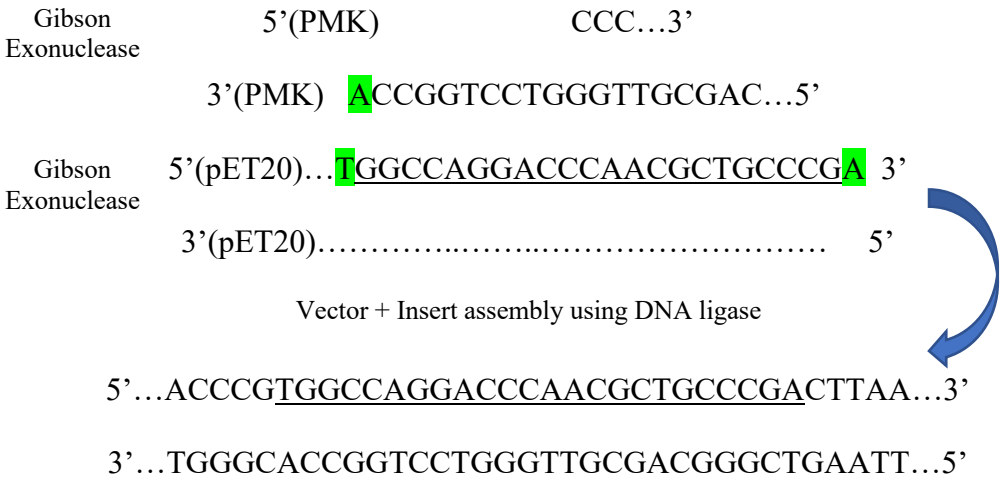

The next step is to derive SP_{141}(2gp8:162 amino acids) and CP (2xyy:430 amino acids) from the data bank. Note that the gene transcription into mRNA starts with a start codon (ATG), and halts at the stop codons (TAA). One start codon (ATG) was inserted at the beginning, and two stop codon (TAATAA) at the end of the gene. Some other critical elements such as the T7 promoter, lac operator, and ribosome binding site (RBS) are also added to the designed gene (the location and number of elements were derived from the duet-vector structure). Remember, the truncated version of scaffolding protein SP_{141} might be utilized with the least effect on the protein assembly process. Each highlighted part stands for an element based on its color as below:

Yellow= cut sites; Purple= T7 Promoter; Green: Start Codon; Red: Stop Codon

ACCGGTGGCCAGGACCCAACGCTGCCCGAGAAATTAATACGACTCACTAT

AGGGGAATTGTGAGCGGATAACAATTCCCCTGTAGAAATAATTTTGTTTAACT

TTAATAAGGAGATATACCATGCGT……

……

……CGCTAATAAGAAATTAAT

ACGACTCACTATAGGGGAATTGTGAGCGGATAACAATTCCCCATCTTAGTAT

ATTAGTTAAGTATAAGAAGGAGATATACATATGGCA……

……

……

……

……CGGTAATAAGCACCACCACCACCACCACCGGT

Also, two restriction cut sites on both sides of each gene (SP and CP individually) were inserted. That way, each gene easily could be removed individually, in case of a non-

functional co-expression system. A potential cause of dysfunctionality in such systems is the high expression of one gene over another. AflII (CTTAAG) and XhoI (CTCGAG) are designated to be placed on both sides of SP_{141} and CP respectively (before T7 promoter and after stop codon). Once digestion with AflII occurs, the gene has the potential to ligate back/ reassemble (using DNA ligation), which leads into SP_{141} elimination. For doing so, an appropriate Gibson overlap is placed right after AflII, at the 3'-end, which is identical to the Gibson homology that was designed earlier (compatible with pET20b/ cut BglII). However, since the 5'-end leaves on a C nucleotide, a single base of C is added to the end of that homology:

ACCGGT**GGCCAGGACCCAACGCTGCCCGA**CTTAAGGAAATTAATACGACT

CACTATAGGGGAATTGTGAGCGGATAACAATTCCCCTGTAGAAATAATTTTG

TTTAACTTTAATAAGGAGATATACCATGCGT……

……

……..…CGCTAATAACTT

AAG**GGCCAGGACCCAACGCTGCCCGAC**GAAATTAATACGACTCACTATAG

GGGAATTGTGAGCGGATAACAATTCCCCATCTTAGTATATTAGTTAAGTATAA

GAAGGAGATATACATATGGCA……

……

……

……

……

……CGGTAATAAGCACCACCACCACCACCACCGGT

Likewise, XhoI is being placed on both sides of the CP. Remember it is considered that, one base to be in common between the XhoI recognition cut site and Gibson homology; that means, on the 5'-end, homology ends up with a C nucleotide which is then taken as the start of CTCGAG. Similarly, for the 3'-end, G nucleotide of homology is taken as the ending base of XhoI:

ACCGGTGGCCAGGACCCAACGCTGCCCGACTTAAGGAAATTAATACGACT
CACTATAGGGGAATTGTGAGCGGATAACAATTCCCCTGTAGAAATAATTTTG
TTTAACTTTAATAAGGAGATATACCATGCGT……
……
……..……CGCTAATAACTT
AAGGGCCAGGACCCAACGCTGCCCGACTCGAGGAAATTAATACGACTCAC
TATAGGGGAATTGTGAGCGGATAACAATTCCCCATCTTAGTATATTAGTTAAG
TATAAGAAGGAGATATACATATGGCA……
……
……
……
……
……CGGTAATAACTCGAGGCCAGGACCCAACGCTGCCCGACGCACC
ACCACCACCACCACCGGT

As it may be clear, a unique Gibson homology of "**GGCCAGGACCCAACGCTGCCCGAC**" is being repeated three times in the context of the gene. This sequence repetition is not optimal in the genetic design, and could raise some potential concerns and issues, about which we will elaborate more in the next chapter.

In the next step two EcoRI restriction cut sites were incorporated right before the CP stop codon. That gives a predefined region to add any switchable tags (e.g. ELPs sequences) with suitable Gibson overlaps (77). These EcoRI cut sites are followed with Gibson homologies compatible with the digested ELPs while $(GVGVP)_X$ was cut with NdeI and BglI on both sides.

ACCGGTGGCCAGGACCCAACGCTGCCCGACTTAAGGAAATTAATACGACT

CACTATAGGGGAATTGTGAGCGGATAACAATTCCCCTGTAGAAATAATTTTG

TTTAACTTTAATAAGGAGATATACCATGCGT……

……

……..……CGCTAATAACTT

AAGGGCCAGGACCCAACGCTGCCCGACTCGAGGAAATTAATACGACTCAC

TATAGGGGAATTGTGAGCGGATAACAATTCCCCATCTTAGTATATTAGTTAAG

TATAAGAAGGAGATATACATATGGCA……

……

……

……CGGTGGGCCACGGCGTGGAATTC

TAATAAGAATTCCTGGTGTCGGCGTGCCGGGCCTCGAGGCCAGGACCCAAC

GCTGCCCGACGCACCACCACCACCACCACCGGT

In the final step, there are two crucial elements, which are necessary to be considered. i) The second stop codon (for CP and after the second EcoRI) was added up, since switching or removing the tag would eliminate the primarily-designed stop codon ii) A "(VPGVG)" downstream of the first EcoRI (right before the stop codon) was added for further experimental analysis.

ACCGGTGGCCAGGACCCAACGCTGCCCGACTTAAGGAAATTAATACGACT

CACTATAGGGGAATTGTGAGCGGATAACAATTCCCCTGTAGAAATAATTTTG

TTTAACTTTAATAAGGAGATATACCATGCGT……

……

……..……CGCTAATAACTT

AAGGGCCAGGACCCAACGCTGCCCGACTCGAGGAAATTAATACGACTCAC

TATAGGGGAATTGTGAGCGGATAACAATTCCCCATCTTAGTATATTAGTTAAG

TATAAGAAGGAGATATACATATGGCA……

……

……

……CGGTGGGCCACGGCGTGGAATTCGTGCCCGGCGTGGGCTAATAAG

AATTCCTGGTGTCGGCGTGCCGGGCTAATAACTCGAGGCCAGGACCCAACG

CTGCCCGACGCACCACCACCACCACCACCGGT

The final stage for the gene design would be codon optimization, using the GeneOptimizer online tool (by Thermo Fisher Scientific) following the order placement of the designed gene through Invitrogen (by Thermo Fisher Scientific).

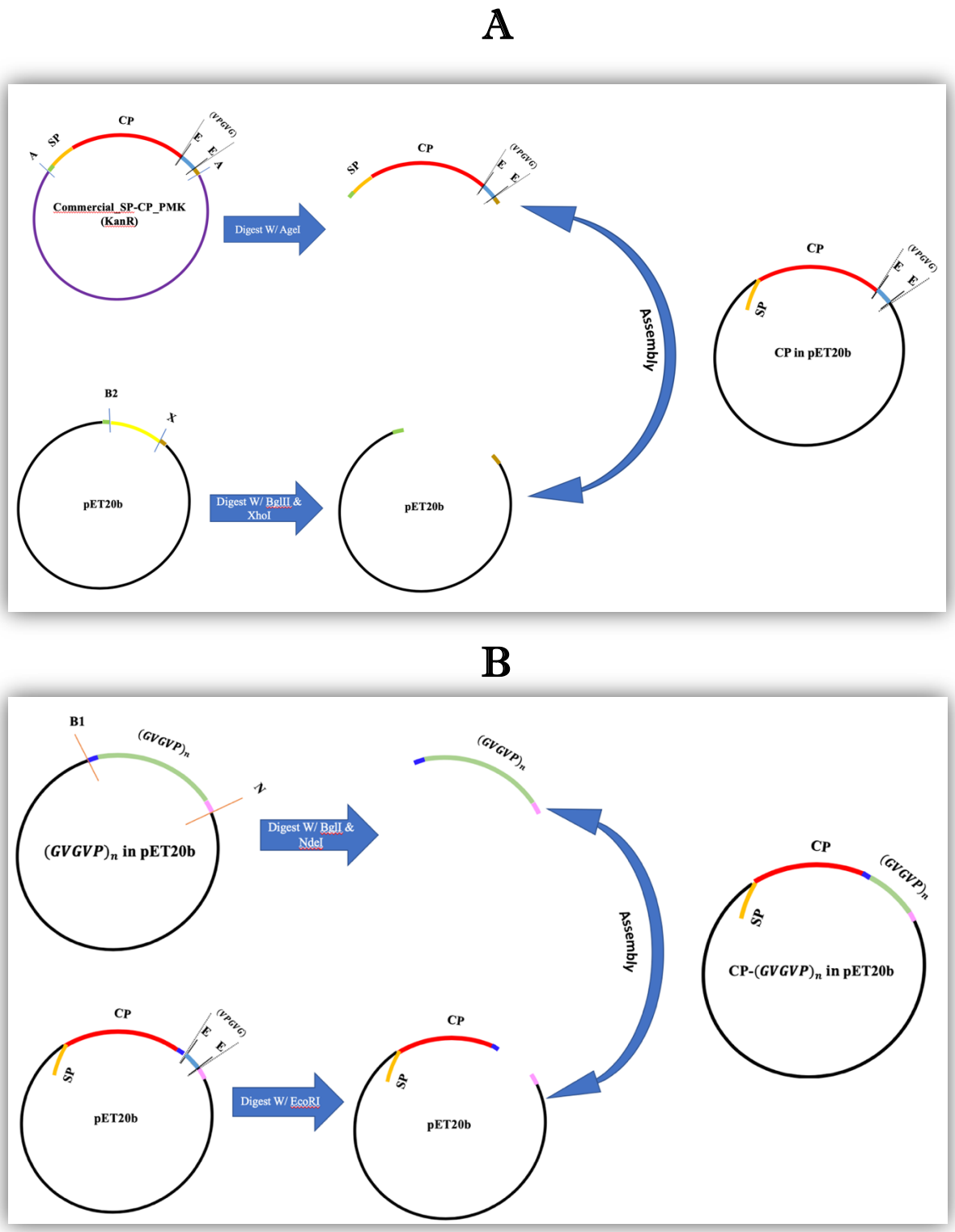

Figure 15. Digestion/ Assembly reactions for ELP-tagged nanoparticle production. A) Cloning reaction; SP_CP Gene subcloning into expression vector pET20b B) Exchanging reaction; to put different tags at C-terminus of the coat protein

2.2. Experimental Preparation

2.2.1. DNA-Prep and Quantification

The SP_CP gene (2181bps) was designed, then ordered from Invitrogen (Figure 16). This commercial gene came in a PMK vector and Kanamycin (KanR) resistance marker. Since PMK is not an expression vector, it was necessary to clone the gene of interest into the pET20b expression vector.

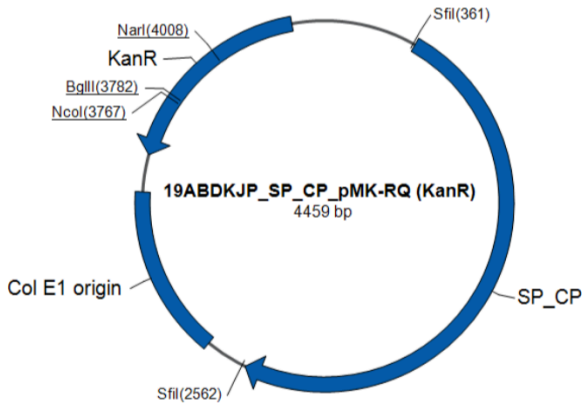

Figure 16. The ordered SP_CP gene in the PMK vector

The ordered-DNA came in a 5 µg-batch, and as a dried powder. After reconstitution to 100 µL with nuclease-free water, the concentration reaches 50 ng/ µL. In the next step, DNA was transformed into Escherichia coli (E. coli) BL21 (strain) competent cells. The transformation process was done by adding 10 pg-100 ng (1 µL of prepared DNA sample) of plasmid within 50 µL of the competent cells using the heat shock technique exactly at $42°C$. The transformation protocol with more details is accessible with details elsewhere (59). Ultimately, the bacteria holding the Kanamycin marker were grown on the kanamycin resistance agar plate. Three individual colonies were picked to inoculate 5 mL of LB-Kan media within the culture tubes.

The day after, all grown bacteria were pelleted to do DNA purification by QIAprep® spin miniprep kit by Qiagen (60) following the DNA sample quantification using Qubit® dsDNA HS assay kit by Invitrogen (61). Concentration measurements showed a low value (in the range of ~1 ng/ µL), but more concentrated DNA is desirable when executing the Gibson assembly experiment. To raise the DNA quantity, the purification step was repeated with $PureYield^{TM}$ plasmid Midiprep System (by Promega) (62). Switching to Midiprep protocol successfully raised the concentration 10-fold (10-20 ng/ µL).

2.2.2. Restriction Digestion and Gibson Assembly

CP-VPGVG

All the reactions that were performed in this section were discussed in the earlier chapter, the genetic design section (**sections 2.1.2. and 2.1.3.**). An aliquot of miniprepped vector (77 ng/ µL) double-digested with BglII and XhoI and miniprepped insert (37 ng/ µL) double-digested with AgeI. Restriction digest reactions were run in PCR-tube for the final volume of 10 µL and 30 µL (vector and insert respectively) following incubation at $37°C$ for 1 h and $65°C$ (heat of inactivation) for 20 min. For the assembly reaction, the digested insert is ligated into the digested vector at the molar ratio of 2:1 using NEBBuilder® HiFi DNA Assembly Master Mix (New England Biolabs) to a final reaction volume of 30 µL, incubating in the thermocycler at $50°C$ for 30 min.

CP-H10, CP-H20, and CP-H40

Once the SP_CP gene was successfully cloned into the expression vector, it might be utilized as a template. This template could undergo a couple of Gibson assembly reactions to add on tags. Previously, $(\boldsymbol{GVGVP})_{\boldsymbol{n}}$ polypeptides with defined numbers of "**n**" were cloned into pET20b in our research group (63). Miniprepped plasmids of

$(GVGVP)_{10}$, $(GVGVP)_{20}$, and $(GVGVP)_{40}$ (all constructs in pET20b vector) were double digested with BglI and NdeI while the vector obtained from the last step (SP-CP in pET20b) was double digested with EcoRI (EcoRI cut sites were used for adding of ELP tags). Three different sets of insert/ digest reactions performed (For three constructs of H10, H20, H40) with the final volume of 20 µL, by incubating for 1 h at 37°C following 20 min at 65°C (heat of inactivation) at the thermocycler. The ligation step was run at the molar ratio of 3:1; insert:vector using NEBBuilder® HiFi DNA Assembly Master Mix (New England Biolabs) for the final reaction volume of 20 µL. The incubation time for this reaction was 30 min at 50°C.

2.2.3. Bacterial Transformation, Culture Prep., and Frozen Stock

Once all gene constructs are cloned within the pET-20b expression vector, it was important to transform those plasmids into Escherichia coli (E. coli)/ BL21 competent cells for the expression. A detailed transformation protocol can be found elsewhere (64).

After the transformation step, bacteria were grown on ampicillin agar plates (as the pET20b vector marker was ampicillin) and incubated at 37°C overnight. The day after individual colonies were picked up (CP-VPGVG: six colonies, CP-H10: six colonies, CP-H20: two colonies, CP-H40: two colonies) by sterile pipette tip. 5 mL of Lysogeny Broth/ LB-amp media (in the culture tube) was inoculated per each colony. The LB-amp media was made by the following recipe: 10 g peptone, 5 g yeast extract, and 5 g NaCl added to 1 L of water, following by mixing and autoclaving the mixture. After cooling down the media (to less than 55°C) 100 mg ampicillin was added to prepare so-called LB-amp media. The growth, was performed on shaking incubator at 37°C and 250 RPM overnight. Next, the DNA for each sample was purified using QIAprep® spin miniprep kit by Qiagen (60).

To prepare a frozen stock of E. coli containing the plasmid of interest properly for long-term usage, the medium was made by mixing 450 µL aliquot of an overnight culture with 450 ul of 40% filtered (0.22 µm) glycerol solution and flash freezing in a dry ice bath (dry ice and ethanol anhydrous). The frozen stock can be useful for making any required overnight cultures of bacteria containing specific DNA for future experiments.

Figure 17. Frozen stock made in the lab

2.2.4. DNA Verification Methods

The purified DNA was analyzed through agarose gel electrophoresis (2%, Invitrogen E-Gel iBase) to verify the expected number of base pairs. If the number of base pairs from the gel would match the expected number of base pairs, the sample will be sent for sequencing (Eurofins).

There are two setup sequencing reactions, one using forward primer and the other one using the backward primer. Each reaction was set by adding 8 µL of the sample (concentration >10 ng/ µL) and 4 µL of primer with the primer concentration of 10 mM. The details about primers are available in table (1).

Primer Name	Oligo Sequence
BglII Forward	5’ ACGACAGGAGCACGATCATG 3’
P20b Reverse	5’ TTGTTAGCAGCCGGATCTCA 3’

Table 1. Primers in use

2.3. Protein Expression and Purification

Different approaches were tested for protein expression and purification (including both failed and successful ones) based on the properties of the constructs. Following is a glance on what has been done in regard.

2.3.1. Induction Versus Auto-Induction Expression and Purification

CP-VPGVG was expressed and purified differently compare to two other constructs of CP-H10 and CP-H40. The detail for such a decision is elaborately discussed in the result and discussion section.

CP-VPGVG

Pipette tips were used to scrape frozen CP-VPGVG stock and inoculate two culture tubes containing 5 mL of LB-amp. These culture tubes were placed on the incubator shaker overnight at 37°C and 200 RPM for 12-16 h. After that time, the content of both culture tubes was poured into an autoclaved Erlenmeyer flask, which was filled with 1 L of LB-amp media to start protein synthesis under an aerobic condition. Expression was induced at mid-log phase/ optical density of 0.8 ($OD_{600} = 0.8$) with isopropyl β-D-thiogalactopyranoside (IPTG) added for a final concentration of 1 mM. After 5 hours of post-induction at the condition of 37°C and 200 RPM, cells were harvested by centrifugation at 4200 RPM for 45 min and finally cell pellets stored at -20 ℃ overnight.

Cell pellets were resuspended in 35 mL of PBS and the mixture was vortexed to get a homogeneous cell suspension. The cell suspension was lysed by the pulse sonicator (Fisher Scientific Sonic Dismembrator 550), at the power level of 10 for 9 runs of 10s on/ 10s off. Due to cell membranes rupturing, the resulting solution contained desired protein.

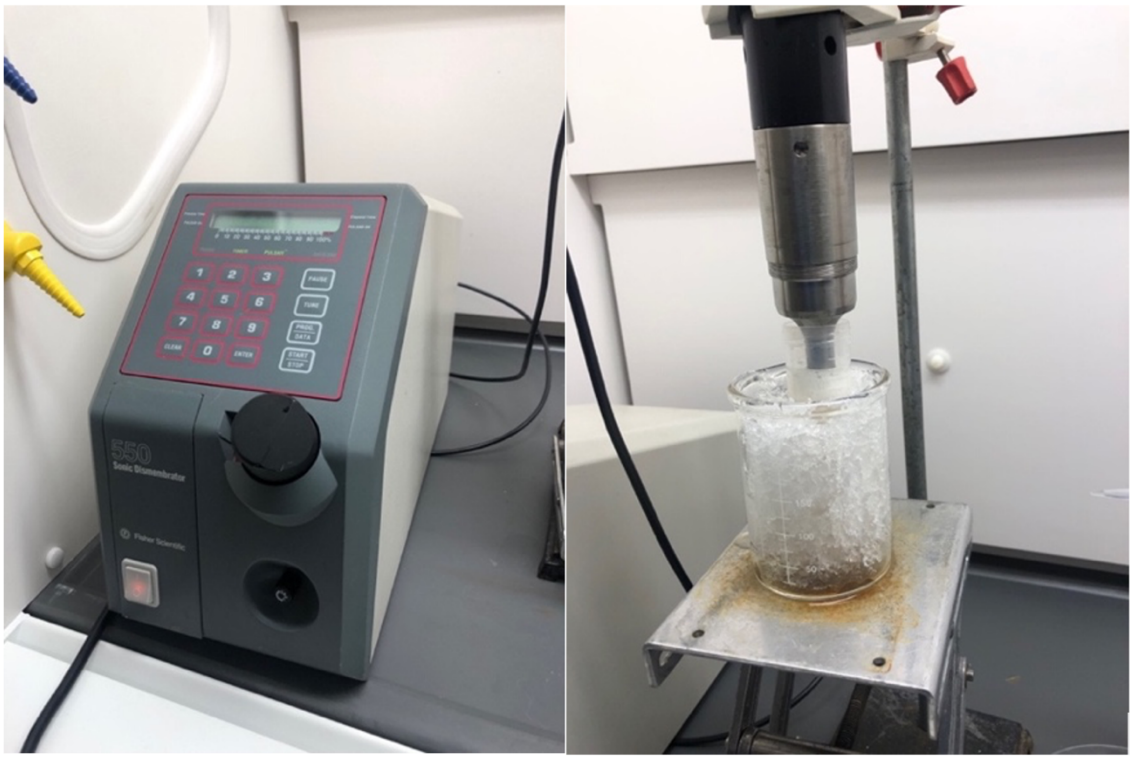

Figure 18. Sonicator for the cell-lysis. The lysate temperature has been regulated by ice to prevent any protein unfolding/ denaturation

The lysate solution was gone through thermal cycling (sequential hot and cold cycles) to purify the protein of interest, based on its phase transitional behavior. The brownish lysate solution was kept on ice for 15 min right after sonication to cool down the solution. A cold centrifugation 10000 RPM run, at $15°C$ for 30 min was performed to separate bacterial waste and cell debris. The supernatant was collected and placed into incubator for the period of 30 min at $60°C$. Since there was no phase separation (the solution was transparent) ammonium sulfate was added to the final concentration of 2 M. Once the phase

separation was observable (forced-salting out), the hot cycle was run for 15 min of 11000 RPM at 40°C. Next, the supernatant was discarded and the pellet was resuspended thoroughly by adding PBS to a final volume of 15 mL (resuspension volume is proportional to the weight of the pellet).

CP-H10 and CP-H40

The overnight cultures for both CP-H10 and CP-H40 were made similar to CP-VPGVG. The content of culture tubes was added into 1L of prepared auto-induction broth (62, Appendix A). Auto-induction expression was done at 25°C and 200 RPM for 30 h. The cells were harvested for one bacterial cycle and stored at -20 ℃ overnight.

Cell pellets were resuspended in 35 mL of PBS. For these two constructs, the power level was set at 7 for 9 runs of 10s on/ 30s off. The brownish lysate solution was cooled down for 15 min on ice right after sonication. A cold centrifugation 10000 RPM run at 15°C for 30 min was performed to separate bacterial cell debris (waste). The supernatant was collected and placed into the incubator for a period of 30 min at 60°C. The phase separation was observable for both constructs however for the CP-H10 the phase separation was not thorough (semi-turbid), so ammonium sulfate was added for the final concentration of 1 M. The rest of the protocol and more details on purification step is accessible on the Appendix B.

2.3.2. Protein Extraction Using B-PER

The desire for a mild method for protein extraction from bacteria instead of mechanical disruption araises whenever the harsh methods would deleteriously impact the structure of studied proteins (e.g. protein aggregation, unfolding, etc.). The method substitution significantly could enhance the protein purity base on the nature of the protein. In this case,

there would be a chance for the aggregation during the purification step (sonication step), due to the particle temperature dependency. Both CP-H10 and CP-H40, that were expressed with the IPTG method, were purified using B-PER as well (parallel to the mechanical approach).

The cold pellets of the expressed proteins (CP-H10 and CP-H40 which were expressed at 37°C and IPTG induction method) were collected and 2 mL of B-PERII reagent was added per gram of each pellet. The tube-content was vortexed until it became homogenous, following incubation for 10-15 min at room temperature. Ultimately, lysate was centrifuged at 15000xg for 5 min. The supernatant might include the revived insoluble proteins (CP-H10 and CP-H40) in the lysate, as the purification approach was changed.

Figure 19. Samples of CP-VPGVG, CP-H10, and CP-H40 were heated up to 60°C which results in clear, semi-turbid, and turbid solutions respectively. Ammonium sulfate. was added to CP-VPGVG and CP-H10 to reach the final concentration of 2 M and 1 M individually and salt out the proteins of interest

2.4. Technical Methods for Synthetic VLP Characterization

2.4.1. UV-VIS Spectroscopy

The first helpful application for UV-VIS spectroscopy is concentration determination. An absorbance (A) measurement, utilizing spectrophotometer plus incorporating the Beer-Lambert law for the concentration calculation is an empirical method of concentration measurement in the laboratory. According to the Beer-Lambert law equation (66):

$$A_{280} = \varepsilon l C$$

A: Absorbance at 280nm

ε: Molar absorption coefficient ($M^{-1}cm^{-1}$)

l: Pathlength/ cuvette length (cm)

C: Protein concentration (M)

By knowing A_{280}, ε, l, one is capable of calculating the concentration (C) for any protein sample, with an unknown concentration. The absorption coefficient value (ε) is a function of three different amino acids of tryptophan, tyrosine, and cystine. Some studies suggest the formula below for ε calculation (66). This formula is applicable for a folded protein in an aqueous solution:

$$\varepsilon(280)\ (M^{-1}cm^{-1}) = (\#Tryptophan) * (5500) + (\#Tyrosine) * (1490) + (\#Cystine) * (125)$$

The second helpful application of sample absorption measurement is transition temperature determination. The instrument measures the absorption at different temperature points and plots absorption versus temperature curve. The dependency of

transition temperature to the sample's concentration is determined by utilizing this methodology.

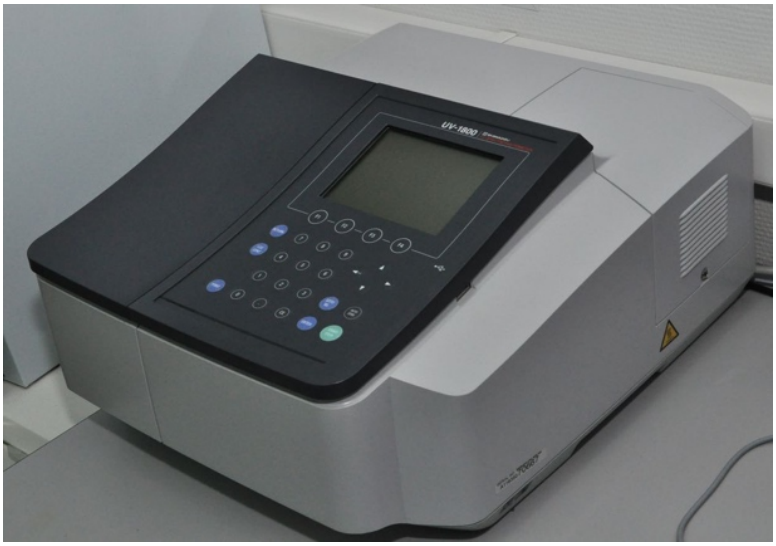

Figure 20. UV-1800, Schimadzu Instrument

Previously, it was shown in a linear chain of an ELP pentapeptide, the transition temperature (T_t) is a linear function of the logarithm of concentration (C) according to the equation below:

$$T_t = T_{cr} - K_c \, ln \, (\frac{C}{C_{cr}}) \quad \text{which} \quad K_c = K_t/\text{L}$$

Where C_{cr} is the critical concentration, K_t is a constant (with the dimension of °C), and L is the number of pentapeptide repeats. Fit parameter values for the linear constructs are shown in the table 2 (63).

Parameter	**Linear ELP**
$\boldsymbol{K_t}$ (°$\boldsymbol{C}$)	114.5
$\boldsymbol{C_{cr}}$ (mM)	30.0
$\boldsymbol{T_{cr}}$ (°$\boldsymbol{C}$)	20.8

Table 2. Linear ELP constructs fit parameters

2.4.2. Dynamic Light Scattering (DLS)

Fixed angle dynamic light scattering is the most common technique for particle size analysis, in the nanometer range. More specifically, this technique is utilized to monitor the average hydrodynamic diameter of formed ELP-tagged particles. Briefly speaking, the philosophy behind the measurement is based on the scattering of the light through the aqueous solution. The light then is scattered by the floating particles from different angles and partially passes through a detector, situated at 173° from the laser source, as it is depicted in Figure 21. Constant monitoring of the light intensity gives a distribution intensity, the software translates that intensity-fluctuations into a correlation function, and after to the diffusion coefficient (D). Finally, the diffusion coefficient could be correlated into the hydrodynamic diameter, using the Stokes-Einstein equation:

$$d(H) = \frac{kT}{3\pi\eta D}$$

Where d (H) is the hydrodynamic diameter, D is the translational diffusion coefficient, K is the Boltzmann's constant, T is the absolute temperature, and η is the viscosity.

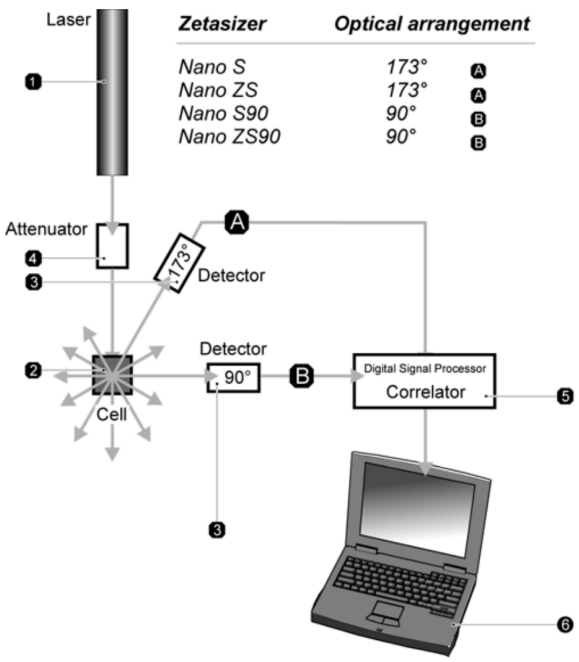

Figure 21. Optical configuration for the Zetasizer (78)

2.4.3. Scanning Electron Microscopy (SEM)

Organic and biological samples are among the most difficult samples to image with SEM, due to their natural non-conductivity and sensitivity to the striking electron beams during the microscopy (75). To find more detail on sample preparation, please refer to **section2.5.4**.

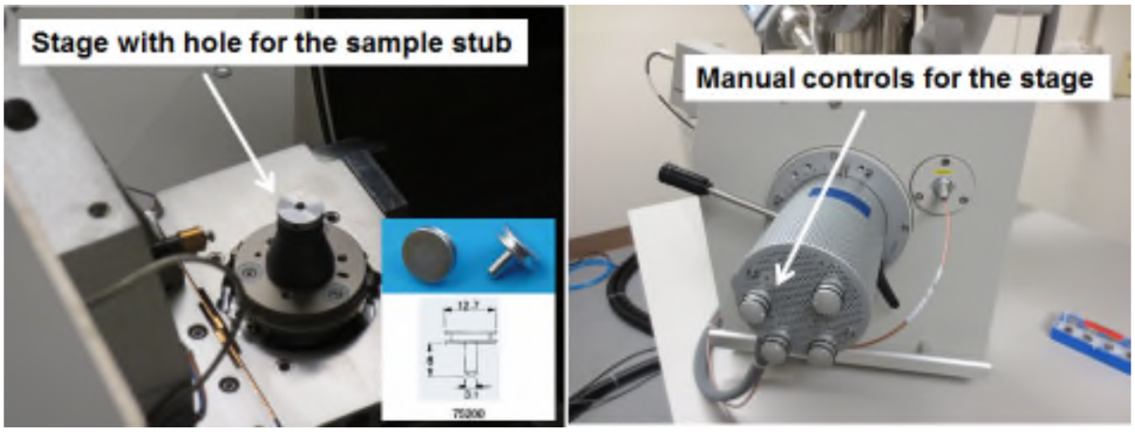

Figure 22. SEM stage and controls. The sample holders are represented in the left figure

2.5. Protein Characterization

2.5.1. SDS-PAGE Gel

Sodium dodecyl sulfate-polyacrylamide gel electrophoresis (SDS-PAGE gel) can be considered as one of the valid characterization tools for the protein's molecular weight verification. SDS-PAGE mini protein gel (4-12% Bolt Bis-Tris, 1 mm, 15-well, Invitrogen) was utilized in these sets of experiments. The sample was prepared, loading up to 0.25 µg of protein max, per each well. The samples were prepared by combining 4 µL of sample reducing agent (10X), 10 µL of LDS sample buffer (4X), desire amount of protein sample, and the rest deionized water to reach a final volume of 40 µL. Samples were boiled in a water-bath at 70°C for 10 min. Samples were loaded into the gel wells and run for 22 min at a constant voltage of 200 V, using MES running buffer. The standard in use was Fisher Brand SeeBlue Plus2 Pre-stained.

2.5.2. UV-VIS Spectroscopy Measurement

The concentration of protein in aqueous solutions is a crucial variable that needs to be determined. To do the measurement a quartz cuvette was filled with 1 mL of PBS to zero the instrument at the absorbance reference point of 280 nm (wavelength), using a Biomate3 system. In the next step, the quartz cuvette was filled with 1 mL original sample (PBS solvent) for the absorbance measurement.

The three amino acids, tryptophan, tyrosine, and cysteine determine the extinction coefficient of the constructs and are only present in the coat protein sequence (and not ELP sequence). Thus, regardless of the arm's length, the extinction coefficient value is identical for all synthesized protein constructs with the value of $\varepsilon = 44920 \mathrm{M}^{-1}\mathrm{cm}^{-1}$. The cuvette

in use has a 1cm length path (the length which laser beam passing through). Knowing those variables, the concentration for each sample can be calculated.

The UV-VIS 1800 (Shimadzu) using its software to create adsorption (turbidity) curve (adsorption versus temperature curve) at a constant 350 nm wavelength. For each curve, a large change in the turbidity of samples was expected as the temperature reached the transition temperature. Once the transition temperature was surpassed (after observing a huge leap around T_t), the testing could be stopped.

Protein solutions were made over a concentration range of 4 μM to 220 μM for H40 and 1 μM to 100 μM for CP-H40, in phosphate buffered saline (PBS) as solvent. The transition graphs were plotted and normalized for different concentrations (Absorbance versus concentration). The transition temperature (in each concentration) was determined by the intercept of the maximum slope and X-axis for each curve. A three-point method was applied to determine this maximum slope and as the result X-intercept. All data were gathered to graph transition temperature versus protein concentration. Finally, the X-axis was converted into the logarithmic scale to obtain a linear trend. In the final step, a linear fit was passed through the data using least-squares method.

2.5.3. Dynamic Light Scattering (DLS) Analysis

The samples were reconstituted to a concentration of 60 μM and pH=6.5 in PBS and then were filtrated through 0.22 μm filters. The quartz cuvette was placed in a Malvern Zetasizer (Nano ZS). A set of experiments for each sample was run including two steps of temperature ramp, i) heating up the samples from 20°C to 70°C ii) cooling down the samples from 70°C to 20°C (samples were CP-H10 and CP-H40). Each point measurement was the average of three different measurements (13x run) and 120s equilibration time right

after each temperature increment step. That equilibration duration gives enough time for the big aggregates to settle (if there are any) as well as reaching to the set temperature. Hence the system is at its equilibrium point while measuring the hydrodynamic diameter.

2.5.4. Sample Preparation for SEM (Scanning Electron Microscopy)

To prepare SEM samples a 20 µL of particle suspension with 12.6 µM in concentration was pipetted onto an autoclaved cover glass. Then the sample dehydrated in ethanol 20%, 40%, 60%, 80%, 100% (v/v), dried at the room temperature, and finally sputter-coated with gold before imaging.

The SPI deposition system was used for the gold sputtering. After attaching a carbon tape on the SEM specimen stub, the sample was fixed on the top of the carbon tape. Next the stub was placed into the chamber including stub holder, glass enclosure, and deposition head. Then, the process included opening the argon valve, switching the "power button" on the SPI Control Module, turning the vacuum pump on, and waiting for 10 min to reach a good vacuum possible (0.2 mbar or less). During this period some turbulence is periodically added to the system, by increasing and decreasing pressure (spinning the valve on the controller). Turbulence and, as the result, convection within the system help a lot with drying the samples off faster and thoroughly. Afterward, the SPI Sputter Module was switched "On" and "Start" button was pressed. The system was set for 10 seconds of sputtering. A reddish-purple glow on the sample is evidence for gold deposition. Then the SPI Sputter Module and SPI Control Module were turned off. Furthermore, the argon valve was closed following vent the chamber by turning counterclockwise the needle valve on the top of the deposition head. Finally, two sides of the silicon chip were dabbed using epoxy to connect the conductivity between the slide and stub. It was allowed to dry for an

hour in room temperature. Right after that time the sample would be ready for the microscopy.

To find out how to set the instrument up for the sample microscopy with SEM, please refer to appendix C.

CHAPTER III

RESULTS AND DISCUSSION

The goal of this project was to develop a temperature-responsive particle system. A single synthetic gene was utilized to produce the base virus like particle (VLP) coat protein subunit and through modification using standard molecular biology and synthetic biology techniques, the genetic code for elastin-like polypeptides (ELPs) with various chain lengths was added into the VLP gene. Two new protein constructs consisting of the coat protein with a C-terminal ELP with 10 and 40 GVGVP repeats (CP-H10 and CP-H40, respectively) were constructed in addition to the CP-VPGVG which was encoded by the original synthetic gene. All of the gene assembly products were verified using DNA sequencing. All synthesized proteins were well-expressed in the bacteria system and were purified successfully. SDS-PAGE was able to verify the molecular weight of each synthesized protein subunit and the formation of the particles was observed utilizing scanning electron microscopy (SEM). The UV-VIS spectroscopy and dynamic light scattering measurements suggested the existence of high-density ELP molecules as well as thermo-reversible behavior of nanoparticles within the system. The effect of ELP chain length on the physicochemical characteristics of this particle was probed.

In summary, the following objectives were completed for this thesis.

i) Developing a meaningful and versatile genetic design that encodes a tagged viral particles.

ii) Expressing and purifying synthesized proteins at a sufficient level.

iii) Characterizing the developed protein constructs with the assistance of some qualitative and quantitative laboratory tools.

3.1. Gene Design Verification

The creation of a building block of synthetic proteins requires the cloning of dual fragment constituted of scaffolding and coat protein genetic codes (SP-CP) within the expression vector. There were couple of bacteria colonies as the result of gene transformation (Figure 23) that were picked up from agar plate for further testing.

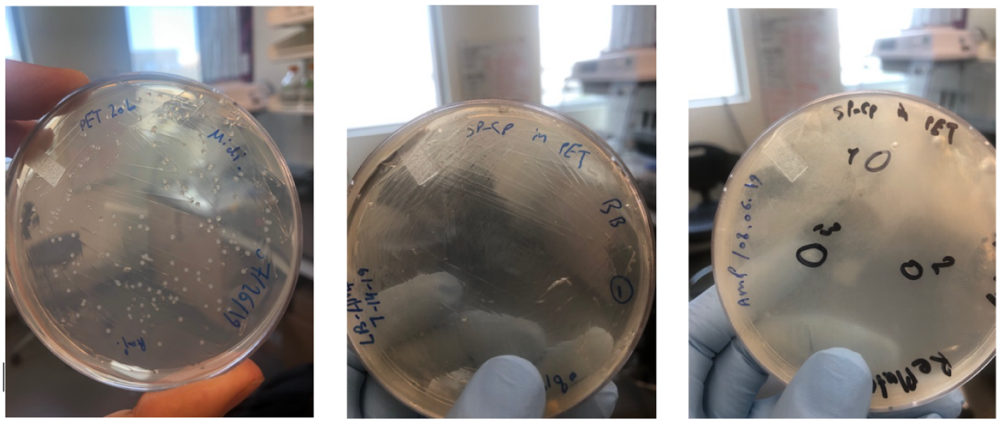

Figure 23. Positive control, negative control, and assembly plates for the SP-CP gene cloned into the pET20b vector. All colonies were grown on the ampicillin agar plates

The result of agarose gel electrophoresis which was run for both digested (negative control) and assembled plasmid is traceable in Figure 24. Out of six studied colonies (lanes of 5, 6, 7, 8, 9, 10), five of them seemed to be undigested (background colonies around), and apparently there was only one successful assembly; lane 7 around 5000 bps.

DNA sequencing results (Eurofins) revealed that only a part of the gene which is responsible for encoding the coat protein (CP) was successfully inserted, and the part responsible for scaffolding protein was not cloned into the pET20b expression vector. It is speculated that this result stems from the sequence of GGCCAGGACCCAACGCTGCCCGA which is repeated three times in the context of the original sequence (at the beginning, near the middle, and at the end). That repetition, statistically would lower the chance of getting the entire SP-CP insert successfully cloned into pET20b via Gibson assembly; in other words, it is probable for the insert to be fused from the other two parts into the vector. However, the experiments were continued with the partially assembled gene, since it was shown (by previous studies), the coat protein itself is enough for the assembly formation even with no scaffolding protein assistance (22). The same verification procedure was applied to the other assembled constructs of CP-H10, CP-H20, and CP-H40. The intact sequences of CP-H10 and CP-H40 were verified by sequencing, whereas CP-H20 assembly was unsuccessful.

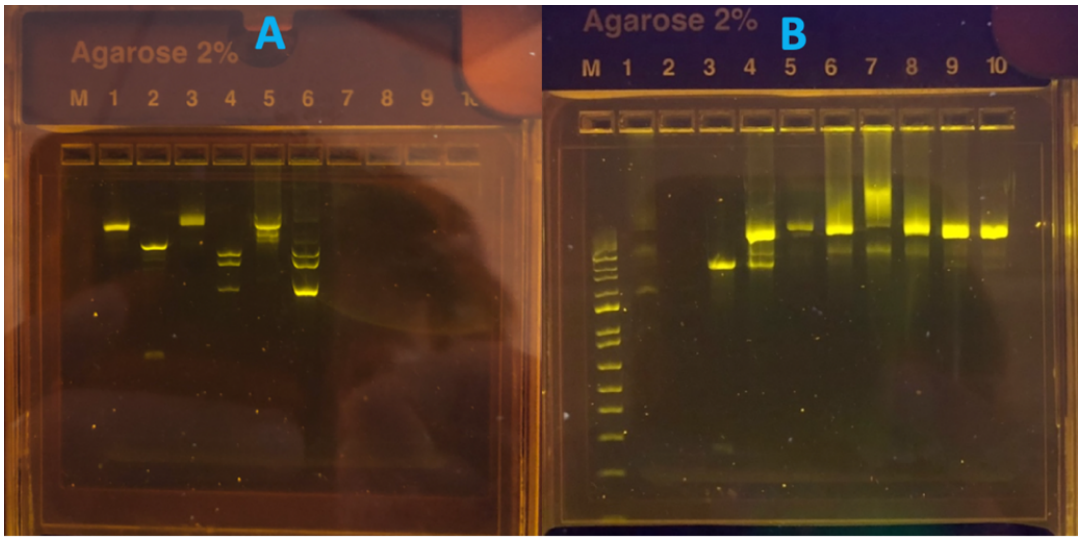

Figure 24. E-gel electrophoresis result A) Digestion verification for miniprepped backbone and insert [1: pET20b, 2: pET20b/XhoI/BglII, 3,5: SP-CP, 4,6: SP-CP/AgeI] B) Assembly verification lane 4 as the positive control (undigested pET20b), the rest of lanes (5, 6, 8, 9, 10) are almost positioned in the same level of positive control except lane 7 (the final assembly expected to have around 5700 bps); [4, 5, 6, 8, 9, 10: undigested pET20b, 7: CP in pET20b]

3.2. Protein Expression and Purification Verification for Different Running Conditions

The three constructs of CP-VPGVG, CP-H10, and CP-H40 were successfully expressed in E. coli induced with IPTG at 37°C as it was confirmed by SDS-PAGE (Figure 25). The bands with red-arrow (lanes 3, 4, 9) are identifying desire expressed proteins CP-VPGVG, CP-H10, CP-H40 with molecular weights of 48.07, 51.45, 63.67 kDa (in their monomeric state) respectively after 5 h of post-induction (before harvesting the cells). Relatively speaking, expressed protein constructs before induction with IPTG following lanes 1, 4, 7 (1:CP-VPGVG, 4:CP-H10, 7:CP-H40) are comparable with those after 2.5 h of post-induction following lanes 2, 5, 7 (2:CP-VPGVG, 5:CP-H10, 8:CP-H40) and after 5 h of post-induction (before cells harvesting) following lanes 3, 6, 8 (3:CP-VPGVG, 6:CP-H10, 8:CP-H40). Even though the post-induction of all constructs resulted in an acceptable

protein amount (compare to pre-induction), the thermal cycling purification has not been successfully performed on CP-H10 and CP-H40 purification. The majority of CP-H10 and CP-H40 were stuck in the first cold pellet (Figure 25, lanes 10 and 12 respectively). Lanes 11 and 13 contain the supernatant of the 3rd cold cycle, which were the purified proteins (CP-H10 and CP-H40 respectively). From the SDS-gel analysis, it is clear that the expression at 37°C with IPTG followed by thermal cycling did not properly purify CP-H10 and CP-H40. Therefore, we considered either altering the physical condition and type of expression or changing the purification method. Lane 14 shows CP-VPGVG of the 3rd cold cycle that is partially purified using 2 M ammonium sulfate.

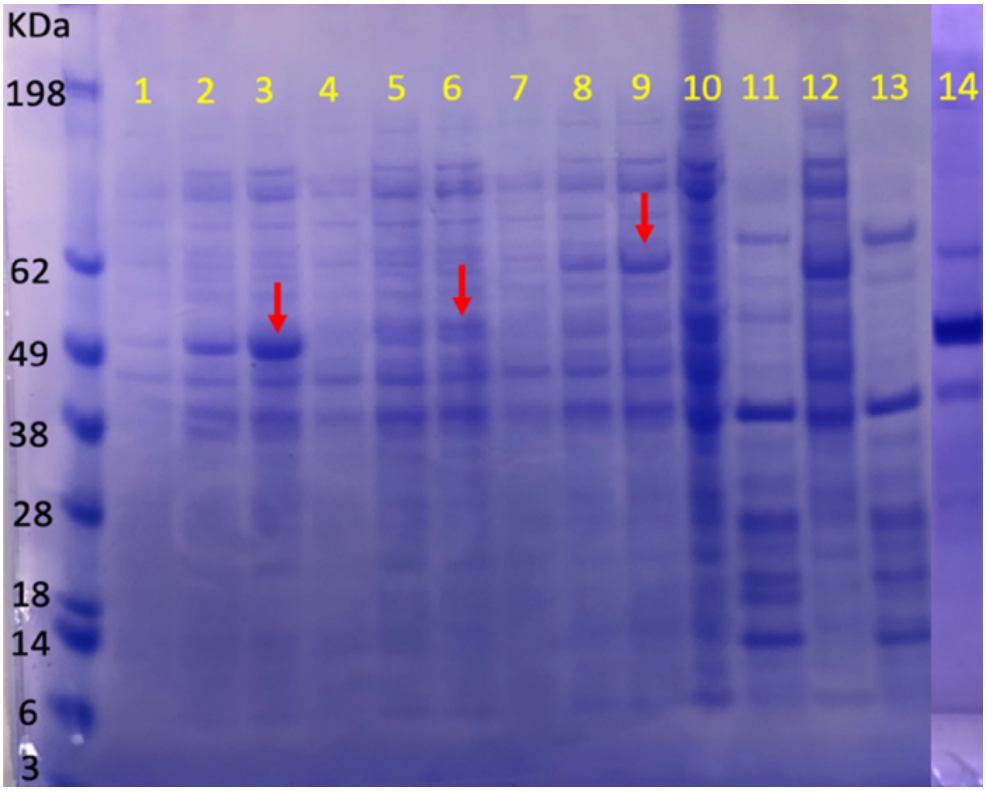

Figure 25. SDS-PAGE gel for IPTG expression/ purification. All CP-VPGVG, CP-H10, and CP-H40 are well-expressed for 5 h of post-induction however CP-H10 and CP-H40 could not be purified. [1, 4, 7: CP-VPGVG, CP-H10, CP-H40 pre-induction; 2, 5, 8: CP-VPGVG, CP-H10, CP-H40 2.5 h post-induction; 3, 6, 9: CP-VPGVG, CP-H10, CP-H40 5 h post-induction; 11, 13: CP-H10, C-H40 (3rd cold- supernatant); 10,12: CP-H10, CP-H40 insoluble fraction (stuck in the first cold pellet); 14: semi-purified CP-VPGVG]

It is assumed purification was not successful due to the particle's aggregation at higher temperatures, going beyond their LCST (lower critical solution temperature) either during the expression or purification step. So, to resolve the issue, it is appropriate to either express the proteins at a lower temperature or use milder alternatives instead of sonication to lyse the cells. The physical condition is switched to 20°C IPTG-induction. Instead of using sonication for purification, B-PER reagent was used as a less severe-temperature method. However, a high fraction of protein was still stuck at first cold pellet step, so using B-PER did not help significantly for the particle's purification.

The formation of inclusion bodies for this particulate protein is also a possibility. To enhance the protein solubility and avoid inclusion body (insoluble fraction) some studies suggested the expression-method alternatives such as auto-induction induction rather than induction with IPTG (67, 68).

This time expression was done by the auto-induction method (without IPTG) method at a lower temperature of 25°C and 200 RPM for 30 h. While the batch was supplied with a well-aerated condition for good bacterial growth. Purified CP-H10 and CP-H40 were found in the supernatant of the 3rd and final cold cycle), as confirmed by SDS-PAGE analysis (Figure 26, lanes 9 and 10). The proteins were successfully purified to an acceptable level for both constructs of CP-H10 and CP-H40.

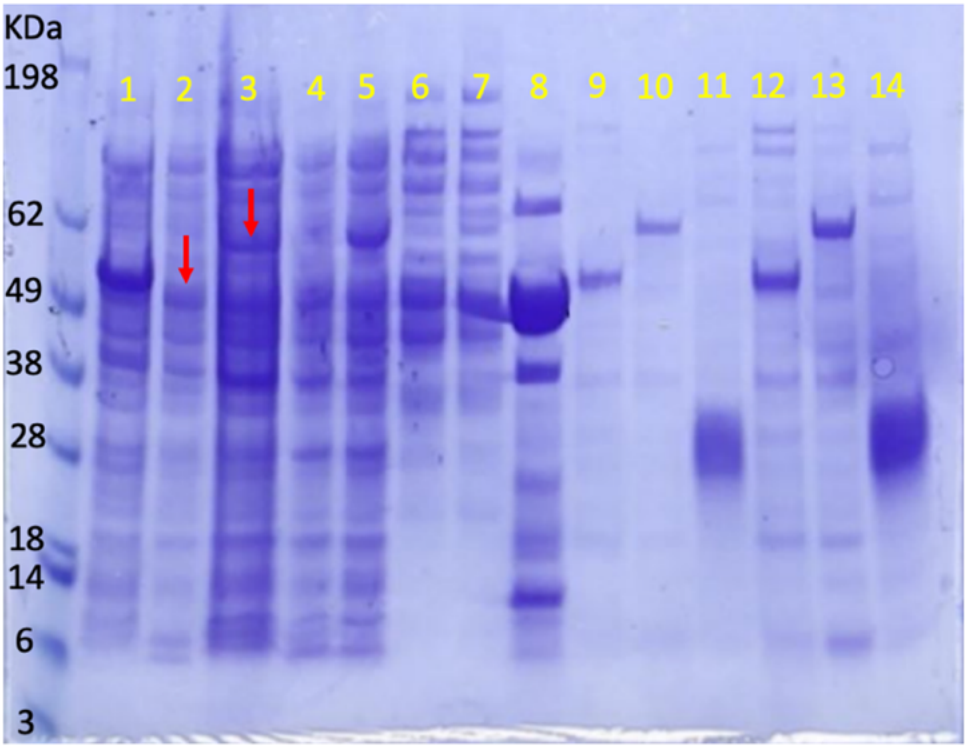

Figure 26. SDS-PAGE gel for non-IPTG expression/ purification Successful purification using altered expression-condition. [2, 3: CP-H10, CP-H40 after 30 h of auto-induction expression at 25°C; (9,12), (10,13): CP-H10, CP-H40 purified and different concentration; 4,5: CP-H10, CP-H40 1st cold pellet; 6,7: CP-H10, CP-H40 2nd cold pellet; 8: CP-VPGVG last supernatant]

3.3. Particles Characterization Using UV-VIS Spectroscopy and DLS

From the data collected and are shown in graphs, a much lower transition temperature was observed for CP-H40 compared to a system of linear ELP with the same number of pentapeptide repetition, H40 (equivalent ELP system), at an equal concentration. This observation could be justified as synthetic VLPs are composed of self-assembling proteins each of which is armed with a polypeptide of interest. Such structure resembles an ELP-dense surface, which potentially turns the particles into a highly robust stimuli-responsive system. This feature potentially makes CP-H40 behave as an ELP system, with a higher molecular weight.

Secondly, the transition temperature is not a big function of concentration in the system of particles as opposed to an equivalent ELP system. That fact also makes sense considering the fact that ELPs with higher molecular weight exhibit less transition temperature (T_t) dependency on concentration changes (70, 71).

Considering those facts, one may tailor the characteristics of the particles (based on the application) by changing the ELP length such that even at lower protein concentrations and lower temperature see the sufficient transition behavior of the particles. However, it would be harder to achieve the transition at lower concentration and lower temperature for the linear ELP system with equal length. For instance, CP-H40 with 1:10 concentration of H40 (CP-H40:H40; 5.5 μM: 55 μM) still has 8°C lower in T_t value (28.54°C: 36.25°C).

The results from UV-VIS, for both CP-H40 and H40, were consistent and show changes in transition temperature, when concentration was changed (Figure 29 and Figure 30). The measured concentration is for the CP-H40 protein, however, since 420 of the protein subunits assemble into a particle, the particle concentration is $1/420^{th}$ the concentration of the protein. However, the calculation of real concentration for the nanoparticle samples is nearly impossible due to limited data that were gathered. Also, the fact that the ratio of molecules in monomeric state and particle state (monomeric: particle) as well as monomodal dispersity of the particles (if all particles are exactly constituted of 420 monomers) are not clear, would add on more complexity for the real particle concentration determination. With that said, we estimate the yield range of 20-30 mg (nominal values) for that system of particles. Despite all of above discussions, the relative comparison of constructs (CP-H40 and H40) remains valid.

The dependency of transition temperature (T_t) to H40 concentration was compared between empirical value and mathematical model in the other studies to ensure the consistency and validity of the experimental data (69, 70). The data that were extracted for the samples obey the proposed mathematical model with a narrow cut-off (empirical T_t have a little lower value than calculated T_t and the slopes are nearly identical). However, the empirical values of T_t for CP-H40 significantly deviated from the mathematical model (with the same amount of pentapeptide) probably due to fulfillment of the named model for prediction of pre-defined structures such as linear ELP, three-armed ELP, etc. and not a spherical ELP-decorated architecture.

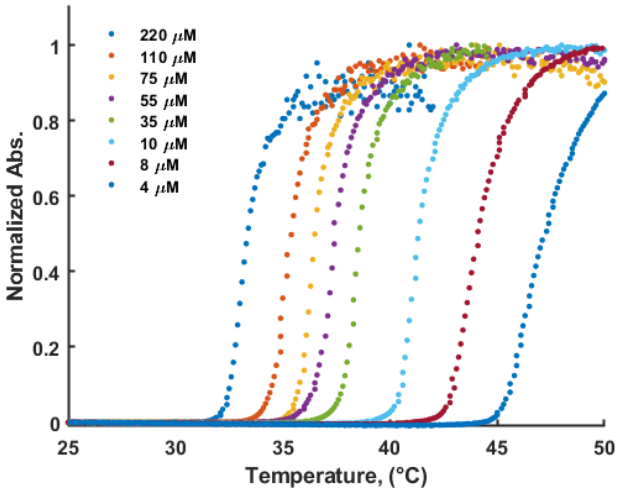

Figure 27. UV-VIS data for H40

Concentration (μM)	220	110	75	55	35	10	8	4
T_t (°C)	32.18	34.23	35.25	36.25	37.51	40.22	42.69	45.04

Table 3. H40 transition temperature correspond to each concentration. A three point and maximum slope method was used to determine T_t (X-intercept)

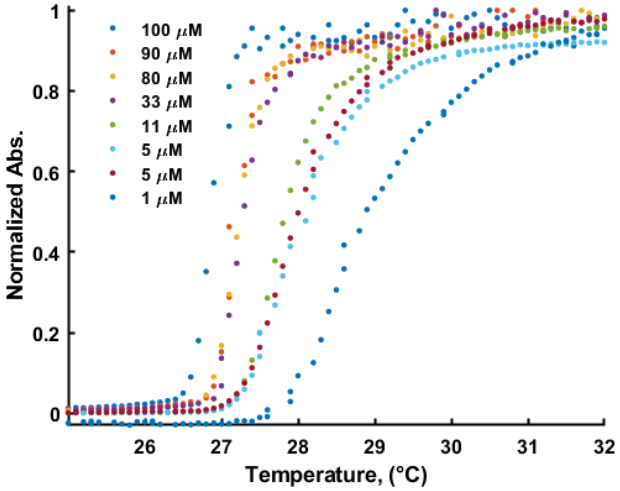

Figure 28. UV-VIS data for CP-H40

Concentration (μM)	100	90	80	33	11	5.5	1
T_t (°C)	32.18	34.23	35.25	36.25	37.51	40.22	42.69

Table 4. CP-H40 transition temperature correspond to each concentration. A three point and maximum slope method was used to determine T_t (X-intercept)

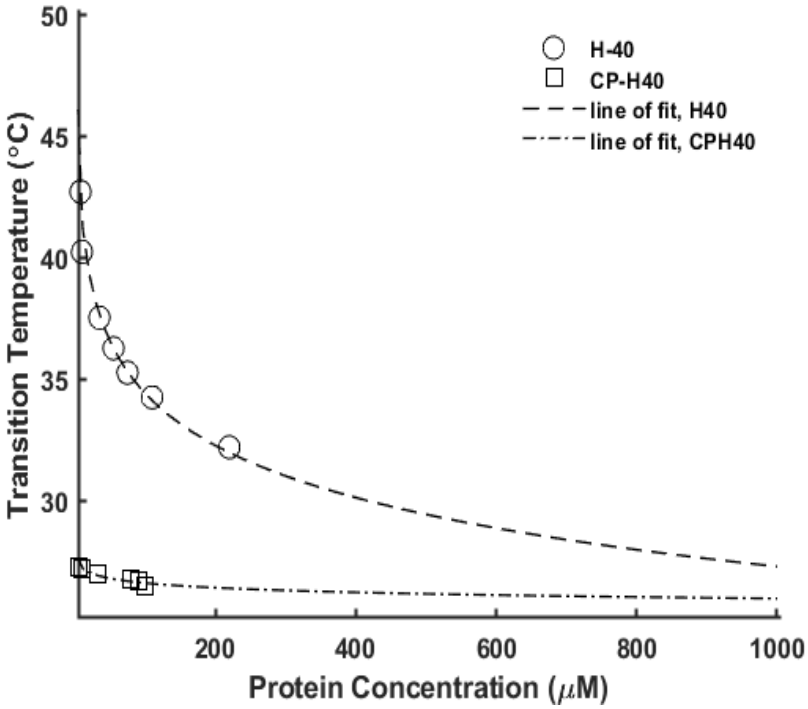

Figure 29. Nonlinear functionality of Transition Temperature versus Concentration

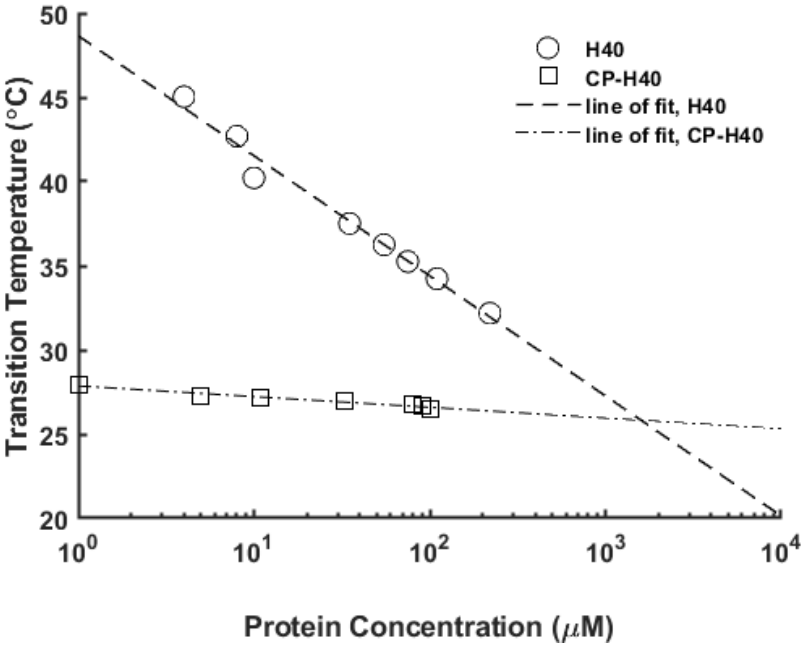

Figure 30. Linear functionality of Transition Temperature versus Concentration

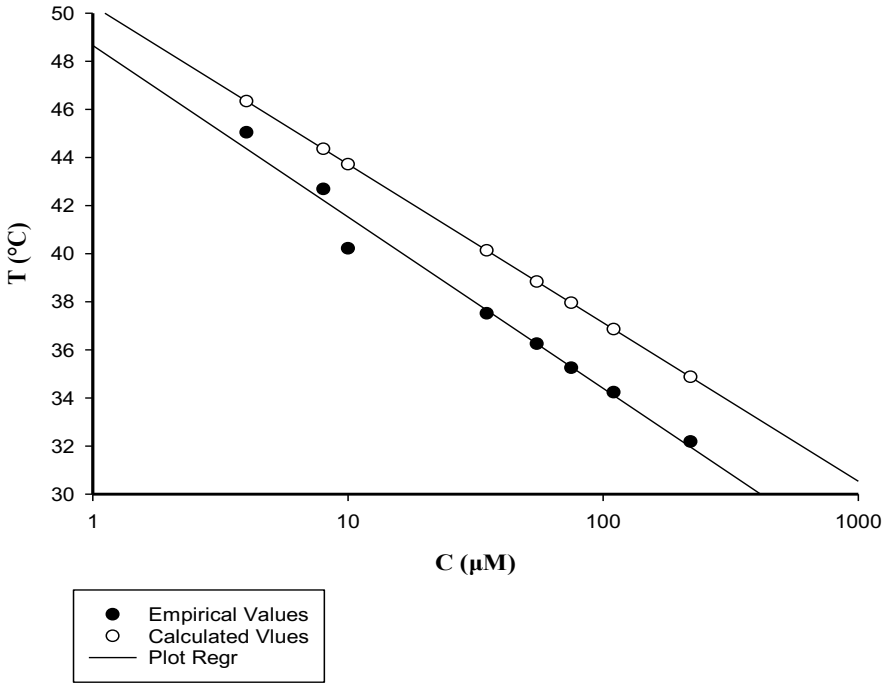

Figure 31. Comparison of calculated data and empirical data for H40

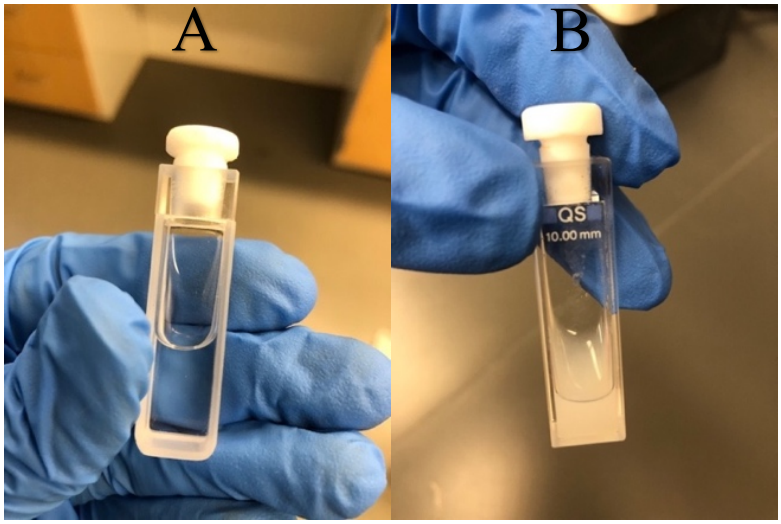

Figure 32. ELP-tagged nanoparticles below and above their transition temperature. A) ELP-tagged nanoparticle solution is limpid and pretty stable below their T_t B) raising the temperature above their T_t forces the particles to aggregate and phase transition which leads to coacervation constitution and the milky solution

In order to complement UV-VIS characterization analysis, dynamic light scattering (DLS) was run to observe particle aggregation above their transition temperatures, to determine their hydrodynamic diameter, and to investigate their thermo-reversibility. The DLS measurement was done for both CP-H10 and CP-H40 constructs. The aggregation of particles from 70 nm to couple hundred nm happened at 50°C and 30°C for CP-H10 and CP-H40, respectively, (Figure 33) which shows that transition temperature is around those values. This is consistent with the UV-VIS data that showed the CP-H40 transition temperature (with an equal concentration) is around 26°C. Another interesting characteristic of these hybrid particles, was their thermo-reversibility behavior. Once the samples were heated up to 70°C, the nanoparticles aggregate to make bigger particles (microparticles 4 to 6 μm in diameter) and as they were cooled down to 20°C, the particles go back to their original diameter due to the thermo-reversibility of the aggregation process.

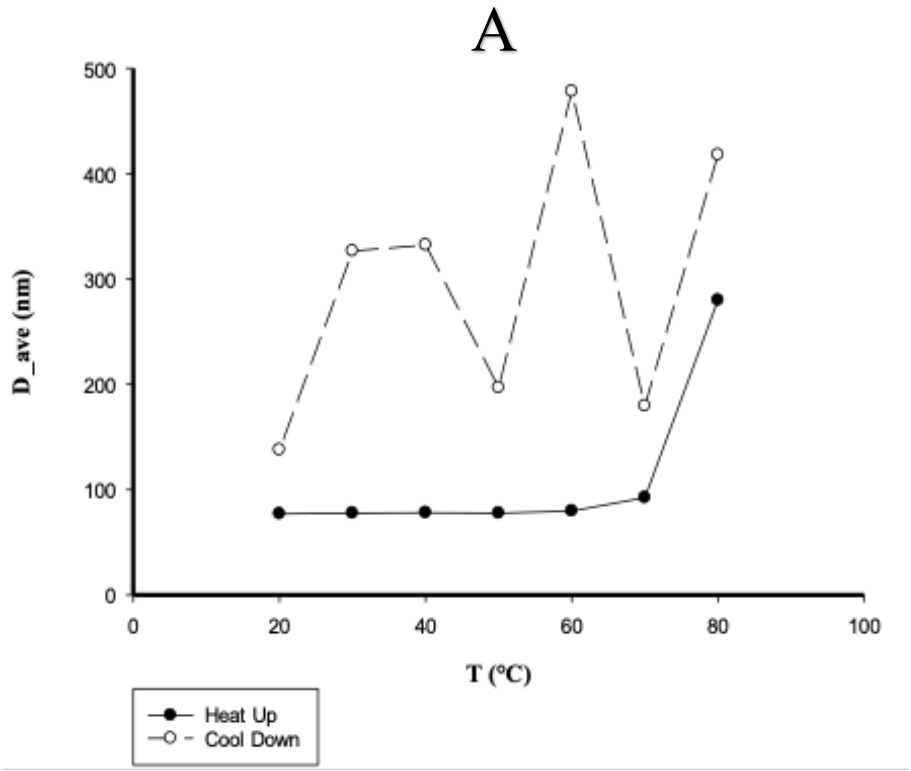

B

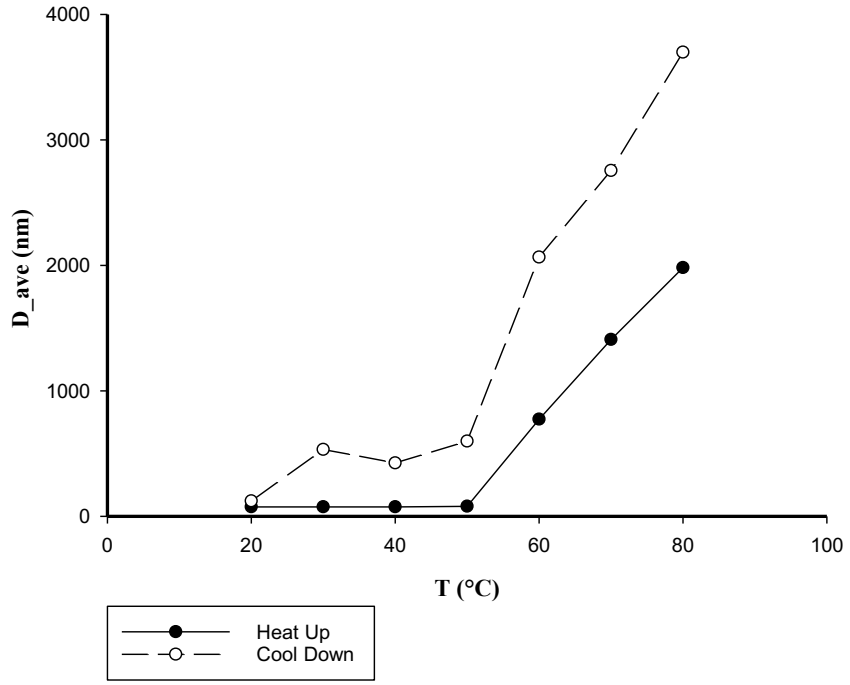

C

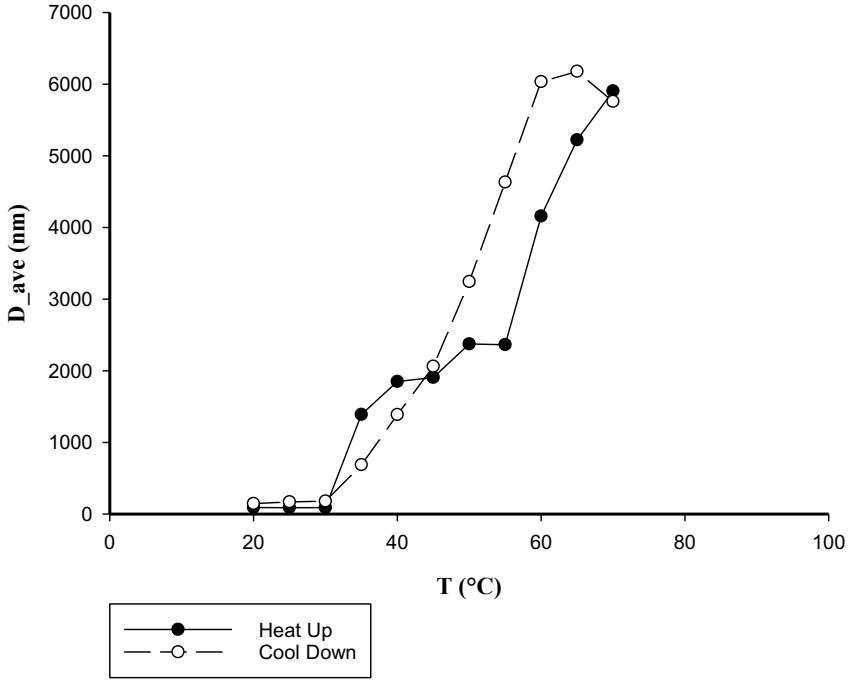

Figure 33. Diameter alteration upon changing the temperature for all constructs of A) CP-VPGVG B) CP-H10 C) CP-H40

A

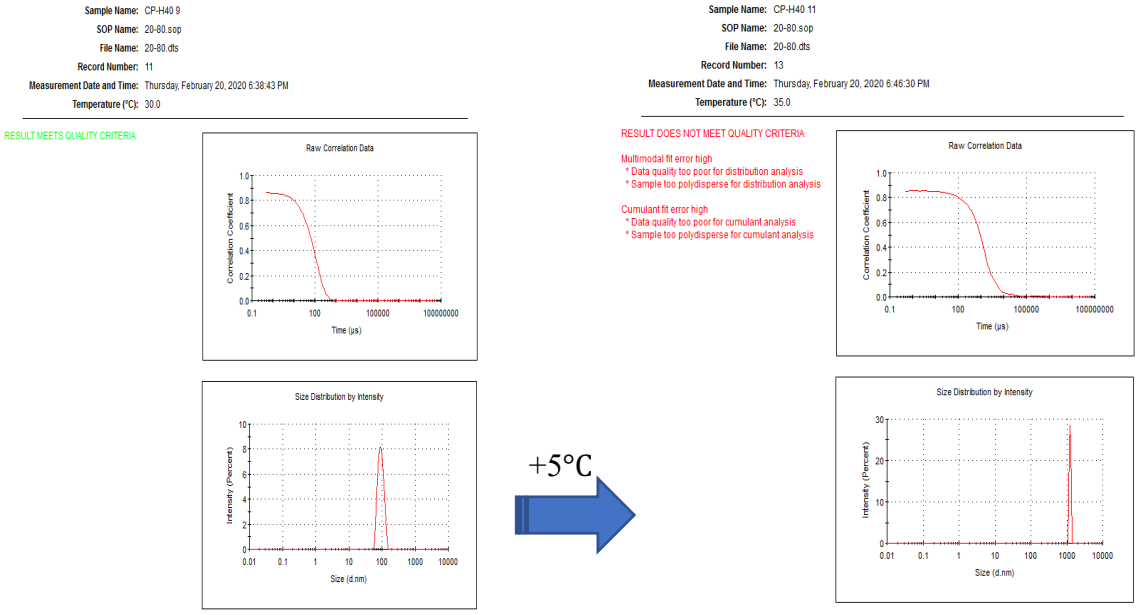

B

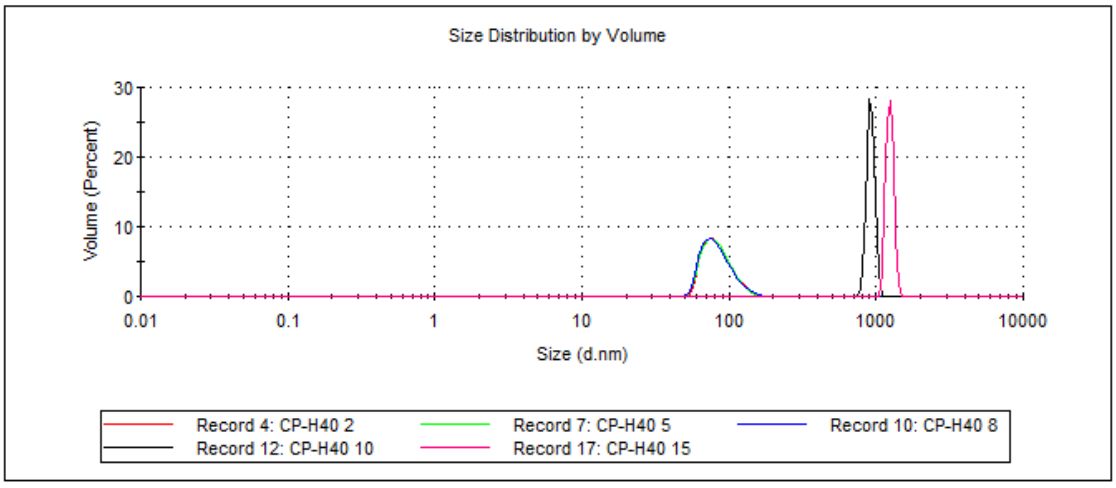

Figure 34. Comparative graphic analysis from DLS measurements for CP-H40 A) As it is observable the sole peak shifted from around 100 nm to 1000 nm increasing the temperature by 5°C (from 30°C to 35°C) B) Size distribution by volume at 30°C, 35°C, and 40°C

3.4. Scanning Electron Microscopy (SEM)

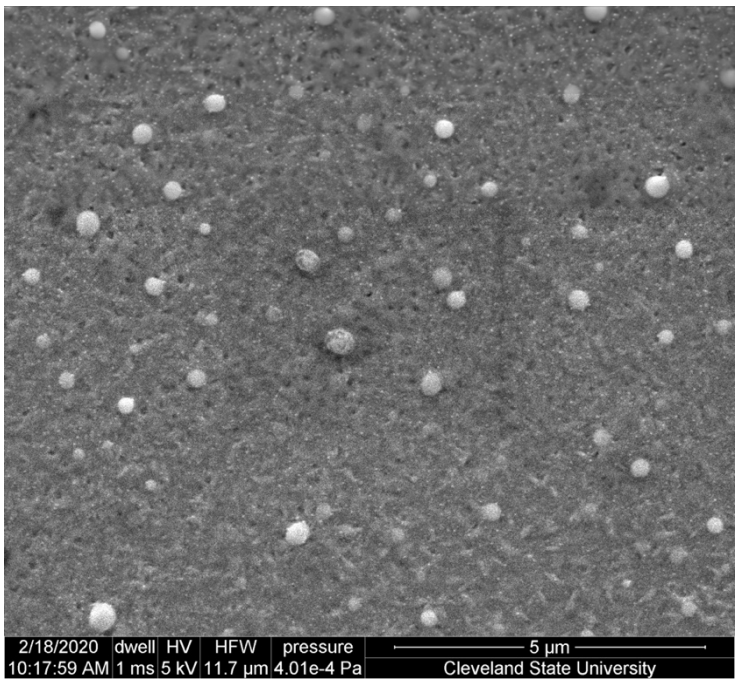

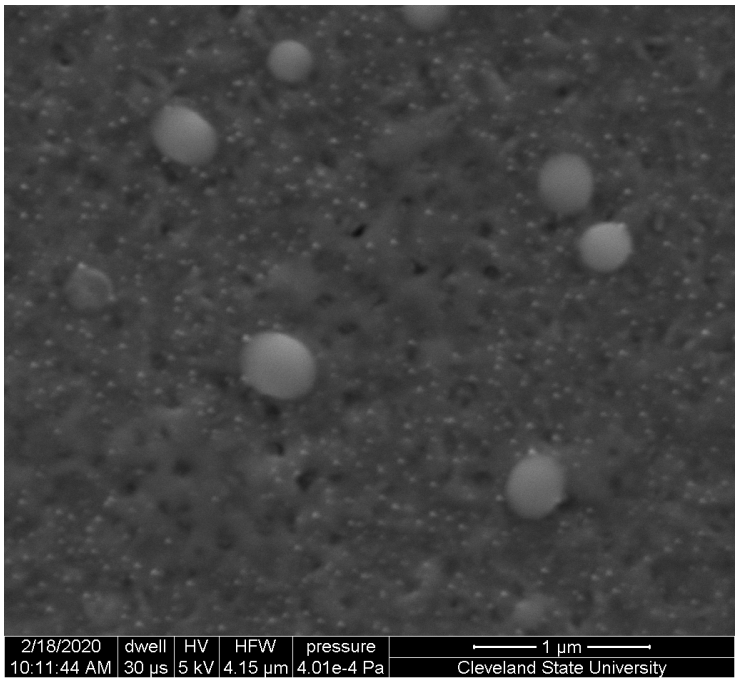

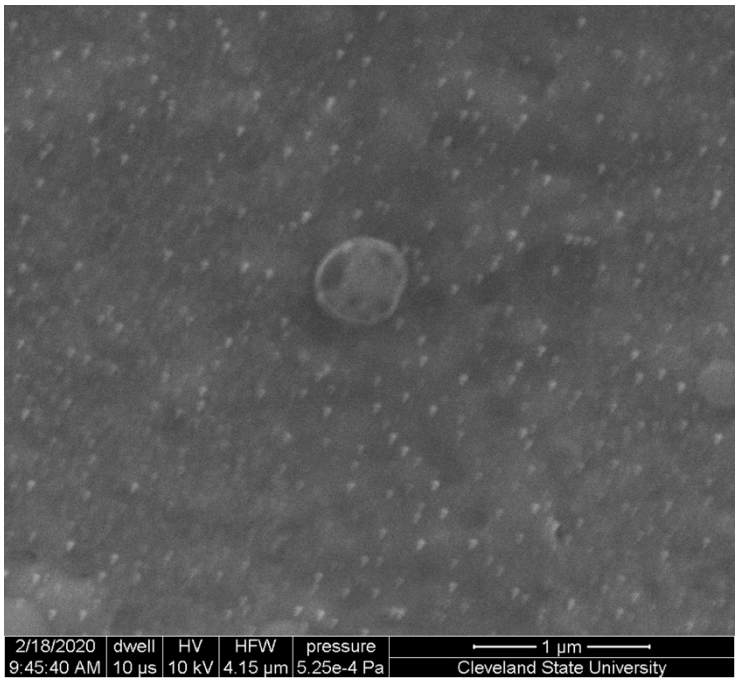

Figure 35. SEM images of modified P22 (CP-H10). Samples were prepared and fixed at the room temperature

The scanning electron microscopy illustrates the generic morphology of the particles. Microscopy was done for CP-H10 samples, while setting different magnification (by zooming in and zooming out). Capturing an image with decent quality was challenging due to the fragility of the particles in the electron beams as well adjusting the instrument to track the particles with such a small diameter.

The particle sizing was analyzed using ImageJ 1.52q. The first step was to fix the scale to 5 µm ~ 5000 nm. From the "Image" drop-down menu Adjust➔ Threshold was selected; The background was adjusted to ensure desire particles were inclusively selected. Once the colors were set up, from the "Analyze" drop-down menu, "analyze particles" was selected. The size was fixed: 0-infinity, circularity: 0.00-1.00, show outlines. The software reports the cross-section area of the particles (Figure 36); consequently, the diameter of particles (in nm) was calculated. Due to poor picture quality and unclean background, all the

particles were not detectable by the software and some dirt was detected as particles. Hence, those particles which were properly detectable by ImageJ are reported. Each of those particles was labeled with an identifier (#), which is attributed to their corresponding diameter (Figure 37). The particles have the range of 100-265 nm in diameter with an average of $\overline{D}$=195.57 nm (195.57 $\pm$ 43.69 nm; mean$\pm$s.d. of the population). The increment in diameter, compared to wild-type capsid size reported elsewhere (71), might arise from a couple of reasons including adding polypeptide arms on the exterior surface of the particles, the sample preparation, and type of microscopy, or even lack of scaffolding protein (SP) within the system.

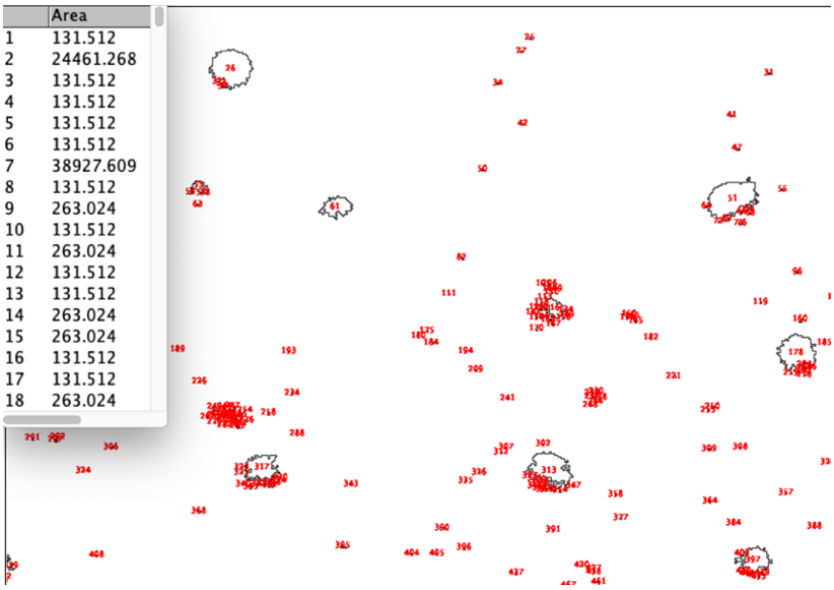

Figure 36. ImageJ software was utilized to analyze the particles size by area calculation

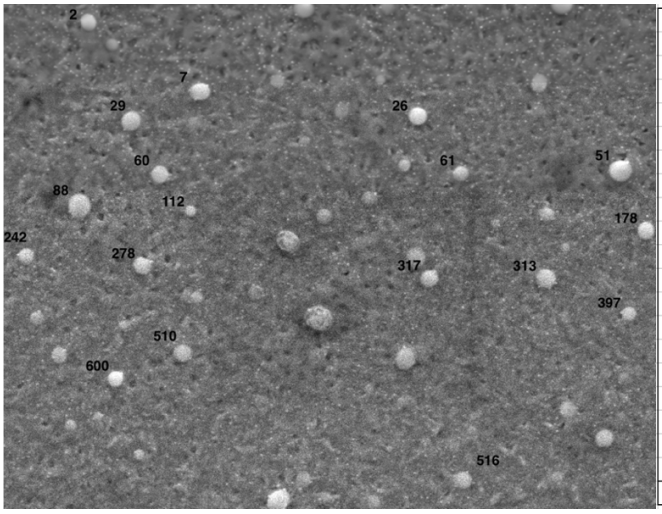

Particle #	Area (nm^2)	D (nm)
2.00	24461.27	176.52
7.00	38927.61	222.69
26.00	49448.58	250.98
29.00	34061.66	208.30
51.00	55498.15	265.89
60.00	28669.66	191.11
61.00	18017.17	151.50
88.00	49317.07	250.65
112.00	8285.27	102.74
178.00	39453.66	224.19
242.00	27354.54	186.67
278.00	33535.61	206.69
313.00	35113.76	211.50
317.00	25118.83	178.88
397.00	18937.76	155.32
510.00	17491.12	149.27
516.00	17096.59	147.58
600.00	45108.68	239.72
Ave.(nm)		195.57

Figure 37. Random particle collection from SEM image for the particle size distribution analysis utilizing ImageJ

Even though the particles were captured using SEM, this type of microscopy is not the most favorable microscopy approach for the representation of viral-like particles. Cryo-transmission electron microscopy (Cryo-TEM) ideally could avoid some of the SEM shortcomings by monitoring the capsid structure at a higher resolution, showing more

details of such structure as well as particle conservation during the microscopy (avoid particle degradation).

3.5. Molecular Modeling

Different molecular structures have been simulated using PyMOL molecular graphics system, version 2.3.5. Such simulations boost our insight for a better understanding of the proteins of interest, structural characteristics at the molecular level, as well as appropriate folding and subunit assembly of the constructs.

Based on what was done in the characterization section including observations, data, and results; likely the synthesized protein of interest (including both coat protein and polypeptide chain) is properly folded. Therefore, these models should accurately represent the system which was developed and show the relative size of the ELP compared to the coat protein.

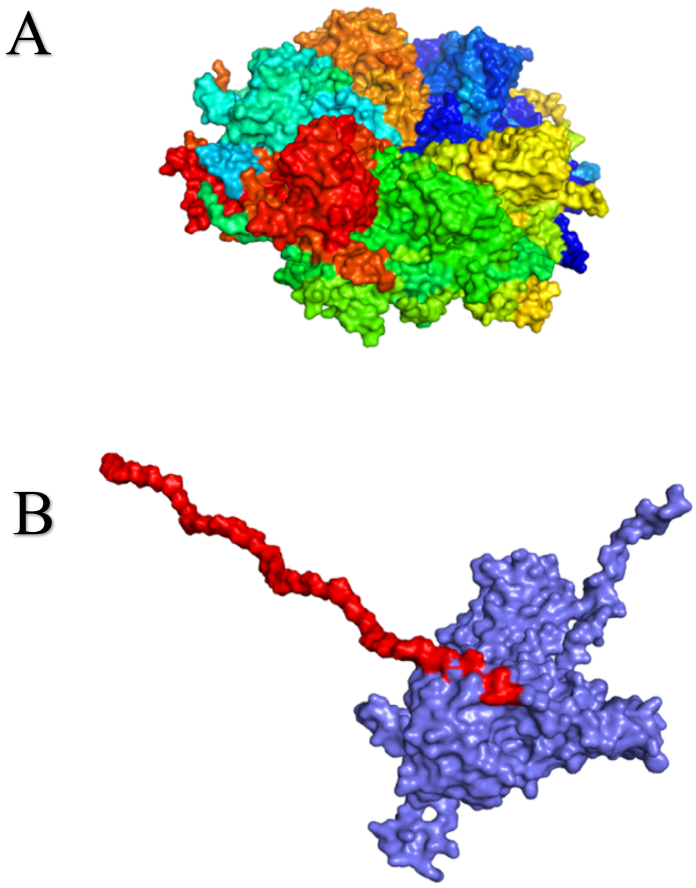

Figure 38. Surface structure demonstration of A) Subunits assembly with symmetrical hexafold axes B) Synthetic CP-VPGVG subunit. The topography (A) clearly shows how structurally monomers are locked into each other, like pieces of a puzzle. The topography (B) demonstrates a well-orientated pentapeptide (red color) attached to the coat protein (CP) monomer's surface (slate color). Figures were prepared using PDB:2XYY

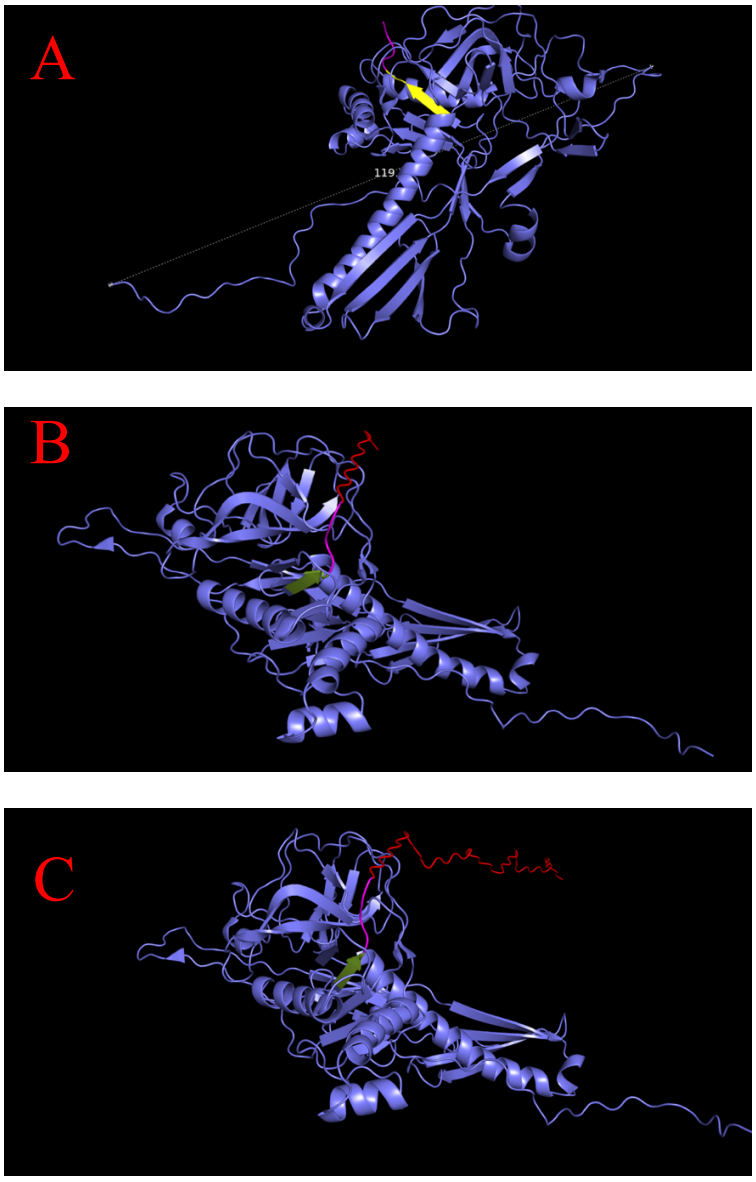

Figure 39. Cartoon structures of A) CP-Wild type B) CP-VPGVG C) CP-H10 the yellow arrow in each schematic is a representation of a unique structure of (GVGLP) which naturally is located at C-terminus of coat protein itself following with the magenta string that represents peptide with the sequence of GQTA and red string that is added ELP polypeptide chain which is fused to the C-terminus of P22 subunit. Each monomer roughly has a length of 119 Å or 11.9 nm base on the results from PyMOL

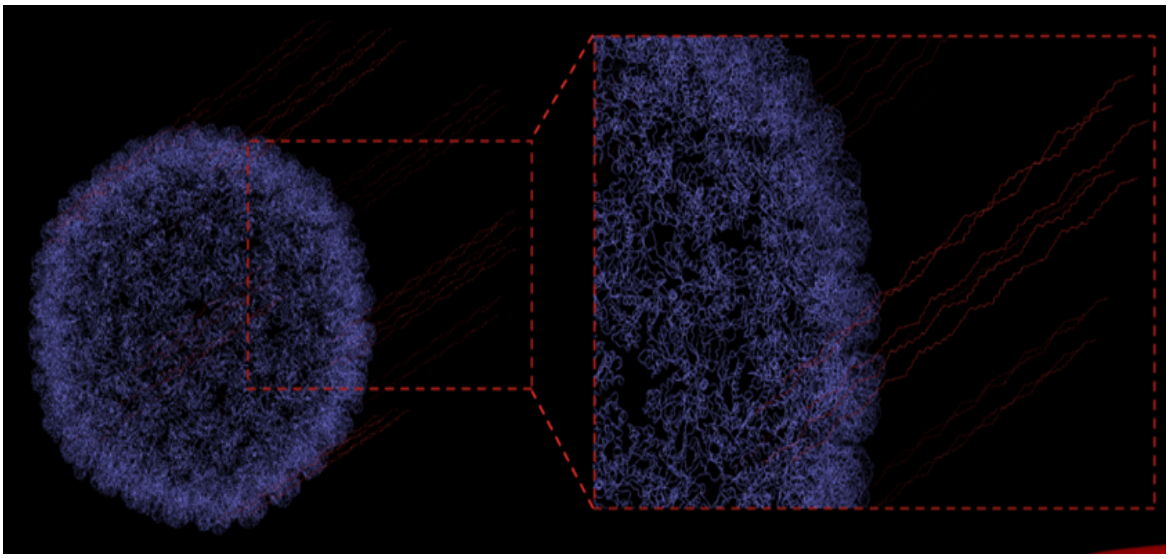

Figure 40. Synthetic CP-H20 nanoparticle assembly

3.6. Future Considerations

- Enhance the purification of constructs with shorter ELP-tag/ no ELP-tag using more advanced purification methods (e.g. SEC chromatography or HPLC)
- Characterization study of particles using other standard methodologies such as cryo-TEM
- Examine expression and assembly of coat protein (CP) in the presence of scaffolding protein (SP) (co-expression with SP)
- Synthesize particles with a broader range of tags and pursue more analysis on the system's parameters (i.e. develop a model for the calculation of transition temperature)
- Do in-vivo study aligned with system's application (i.e. cytotoxicity assay)
- Modify the attached tags to add some functional properties (i.e. adding cell-penetrating peptide sequence to the ending of each tag)
- Conformational and stability study of built-up constructs in various physicochemical conditions (i.e. different temperatures, pH, salt concentration)

CHAPTER IV

CONCLUSION

Introducing a novel ELP-fused nanoparticle platform with functional characteristics was the primary achievement in the scope of this project. After designing ELP-decorated VLPs, the proteins were expressed and purified successfully. It was also demonstrated that nanomaterials with such structures are thermo-reversible.

The high-density ELP pentapeptides on the nanosphere structure mimicked the thermal response of ELPs with a much higher length. This reduction in transition temperature (T_t) stems from the high local density of ELPs on the exterior circumference of each particle due to the highly repetitive array of such structure (i.e. they have low T_t values which are less dependent on temperature). Finally, scanning electron microscopy of VLPs is evidence on the polydisperse system of particles with a range of sizes.

ELP-based drug carriers opened up their own way toward preliminary clinical trials having two main characteristics of i) Well-tolerated in the human body, and ii) Do not trigger significant immune responses in most individuals (74). We are speculating these two main characteristics could be potential function of the proposed system in this study. However, further investigations as proof of concept are needed to be done for such a system in future studies.

Construct Name	Amino Acid Sequence	Molecular Weight (kDa)
(SP)141	MRSNAVAEQGRKTQEFTQQSA QYVEAARKHYDAAEKLNIPDY QEKEDAFMQLVPPAVGADIMR LFPEKSAALMYHLGANPEKAR QLLAMDGQSALIELTRLSERLT LKPRGKQISSAPPADQPITGDVS AANKDAIRKQMDAAASKGDV ETYRKLKAKLKGIR	18.011
CP-VPGVG	MALNEGQIVTLAVDEIIETISAI TPMAQKAKKYTPPAASMQRSS NTIWMPVEQESPTQEGWDLTD KATGLLELNVAVNMGEPDNDF FQLRADDLRDETAYRRRIQSAA RKLANNVELKVANMAAEMGS LVITSPDAIGTNTADAWNFVAD AEEIMFSRELNRDMGTSYFFNP QDYKKAGYDLTKRDIFGRIPEE AYRDGTIQRQVAGFDDVLRSP KLPVLTKSTATGITVSGAQSFK PVAWQLDNDGNKVNVDNRFA TVTLSATTGMKRGDKISFAGV KFLGQMAKNVLAQDATFSVVR VVDGTHVEITPKPVALDDVSLS PEQRAYANVNTSLADAMAVNI LNVKDARTNVFWADDAIRIVS QPIPANHELFAGMKTTSFSIPDV GLNGIFATQGDISTLSGLCRIAL WYGVNATRPEAIGVGLPGQTA GDLGHGVEFVPGVG	48.073
CP-H10	MALNEGQIVTLAVDEIIETISAI TPMAQKAKKYTPPAASMQRSS NTIWMPVEQESPTQEGWDLTD KATGLLELNVAVNMGEPDNDF FQLRADDLRDETAYRRRIQSAA RKLANNVELKVANMAAEMGS LVITSPDAIGTNTADAWNFVAD AEEIMFSRELNRDMGTSYFFNP QDYKKAGYDLTKRDIFGRIPEE AYRDGTIQRQVAGFDDVLRSP KLPVLTKSTATGITVSGAQSFK PVAWQLDNDGNKVNVDNRFA TVTLSATTGMKRGDKISFAGV KFLGQMAKNVLAQDATFSVVR VVDGTHVEITPKPVALDDVSLS PEQRAYANVNTSLADAMAVNI LNVKDARTNVFWADDAIRIVS QPIPANHELFAGMKTTSFSIPDV GLNGIFATQGDISTLSGLCRIAL WYGVNATRPEAIGVGLPGQTA GDLGHGVGVPGVGVPGVGVP GVGVPGVGVPGVGVPGVGVP GVGVPGVGVPGVGVP	51.33

CP-H40	MALNEGQIVTLAVDEIIETISAI TPMAQKAKKYTPPAASMQRSS NTIWMPVEQESPTQEGWDLTD KATGLLELNVAVNMGEPDNDF FQLRADDLRDETAYRRRIQSAA RKLANNVELKVANMAAEMGS LVITSPDAIGTNTADAWNFVAD AEEIMFSRELNRDMGTSYFFNP QDYKKAGYDLTKRDIFGRIPEE AYRDGTIQRQVAGFDDVLRSP KLPVLTKSTATGITVSGAQSFK PVAWQLDNDGNKVNVDNRFA TVTLSATTGMKRGDKISFAGV KFLGQMAKNVLAQDATFSVVR VVDGTHVEITPKPVALDDVSLS PEQRAYANVNTSLADAMAVNI LNVKDARTNVFWADDAIRIVS QPIPANHELFAGMKTTSFSIPDV GLNGIFATQGDISTLSGLCRIAL WYGVNATRPEAIGVGLPGQTA GDLGHGVGVPGVGVPGVGVP GVGVPGVGVPGVGVPGVGVP GVGVPGVGVPGVGVPGVGVP GVGVPGVGVPGVGVPGVGVP GVGVPGVGVPGVGVPGVGVP GVGVPGVGVPGVGVPGVGVP GVGVPGVGVPGVGVPGVGVP GVGVPGVGVPGVGVPGVGVP GVGVPGVGVPGVGVPGVGVP GVGVPGVGVPGVGVPGVGVP GVGVP	63.61

Table 5. Sequences of synthesized proteins

BIBLIOGRAPHY

1. Steinmetz NF, Manchester M. Viral nanoparticles: Tools for materials science and biomedicine, (2011).
2. C. M. Shepherd et al., VIPERdb. a relational database for structural virology. Nucleic Acids Res. 34, D386, (2006).
3. Y. Zhu, B. Carragher, D. J. Kriegman, R. A. Milligan, C. S. Potter, J. Struct. Biol. 135, 302, (2001).
4. Bamford DH, Grimes JM, Stuart DI. What does structure tell us about virus evolution? Current Opinion in Structural Biology. 15(6):655-63, (2005).
5. Suttle, C. Viruses in the sea. Nature 437, 356-361, (2005).
6. Urry DW, Shaw RG, Prasad KU. Polypentapeptide of elastin: Temperature dependence of ellipticity and correlation with elastomeric force. Biochemical and Biophysical Research Communications. 130(1):50-7, (1985).
7. Urry DW. Free energy transduction in polypeptides and proteins based on inverse temperature transitions. Progress in Biophysics and Molecular Biology. 57(1):23-57, (1992).
8. Hull R. Nomenclature and Classification of Plant Viruses. p. 13-45, (2002).
9. Douglas T, Young M. Viruses. Making Friends with Old Foes. Science, (2006).
10. Kang S & Douglas T. Some enzymes just need a space of their own. Science 327, 42–43, (2010).
11. Udit, Andrew K., ed. Protein Scaffolds: Design, Synthesis, and Applications. Humana Press, (2018).
12. Suttle CA. Viruses in the sea. Nature.437(7057):356-61, (2005).

13. Fischlechner, M., Reibetanz, U., Zaulig, M., Enderlein, D., Romanova, J., Leporatti, S., Moya, S., and Donath, E. Fusion of enveloped virus nanoparticles with polyelectrolyte-supported lip, (2007).

14. Toellner, L., Fischlechner, M., Ferko, B., Grabherr, R. M., and Donath, E. Virus-coated layer-by-layer colloids as a multiplex suspension array for the detection and quantification of virus-specific antibodies, Clin. Chem., 52(8), 1575–1583, (2006).

15. Johnson, J. E., and Speir, J. A. Quasi-equivalent viruses: a paradigm for protein, (1997).

16. Zhang Y, Fu J, Chee SY, Ang EX, Orner BP. Rational disruption of the oligomerization of the mini-ferritin E. coli DPS through protein-protein interface mutation. Protein Science. 20:1907-17, (2011).

17. Parent KN, Sinkovits RS, Suhanovsky MM, Teschke CM, Egelman EH, Baker TS. Cryo-reconstructions of P22 polyheads suggest that phage assembly is nucleated by trimeric interactions among coat proteins. Phys Biol. 7(4):045004-, (2010).

18. Wang Q, Lin T, Johnson JE, Finn M. Natural supramolecular building blocks: cysteine-added mutants of cowpea mosaic virus. Chemistry & biology. 9(7):813-9, (2002).

19. Flenniken ML, Willits DA, Brumfield S, Young MJ, Douglas T. The Small Heat Shock Protein Cage from Methanococcus jannaschii Is a Versatile Nanoscale Platform for Genetic and Chemical Modification. Nano Letters. 3(11):1573-6, (2003).

20. Manchester M, Steinmetz NF, editors. Viruses and Nanotechnology. Current Topics in Microbiology and Immunology. Springer Berlin Heidelberg; Available from: http://dx.doi.org/10.1007/978-3-540-69379-6, (2009).

21. Motwani T, Teschke CM. Architect of Virus Assembly: the Portal Protein Nucleates Procapsid Assembly in Bacteriophage P22. J Virol. 93(9):e00187-19, (2019).

22. Suhanovsky MM, Teschke CM. Bacteriophage P22 capsid size determination: Roles for the coat protein telokin-like domain and the scaffolding protein amino-terminus. Virology. 417(2):418-29, (2011).

23. Parker MH, Prevelige PE. Electrostatic Interactions Drive Scaffolding/Coat Protein Binding and Procapsid Maturation in Bacteriophage P22. Virology. 250:337-49, (1998).

24. Padilla-Meier GP, Gilcrease EB, Weigele PR, Cortines JR, Siegel M, Leavitt JC, et al. Unraveling the role of the C-terminal helix turn helix of the coat-binding domain of bacteriophage P22 scaffolding protein. J Biol Chem. 287(40):33766-80, (2012).

25. O'Neil A, Reichhardt C, Johnson B, Prevelige P, Douglas T. Genetically Programmed In Vivo Packaging of Protein Cargo and Its Controlled Release from Bacteriophage P22. Angewandte Chemie (International ed in English). 50:7425-8, (2011).

26. M. van de Waterbeemd, A. Llauro, J. Snijder, A. Valbuena, A. Rodriguez-Huete, M.A. Fuertes, P.J. de Pablo, M.G. Mateu, A.J.R. Heck, Structural Analysis of a Temperature Induced Transition in a Viral Capsid Probed by HDX-MS., Biophys. J. 112 1157–1165, (2017).

27. Urakami A, Sakurai A, Ishikawa M, Yap ML, Flores-Garcia Y, Haseda Y, et al. Development of a Novel Virus-Like Particle Vaccine Platform That Mimics the Immature Form of Alphavirus. Clin Vaccine Immunol. 24(7):e00090-17, (2017).

28. M. Tatnall, J. King, Purification of the Coat and Scaffolding Procapsids of Bacteriophage Proteins from, 547 529-547, (1981).

29. S. Casjens, M.B. Adams, C. Hall, J. King, Autogenous Modulation of Bacteriophage, 123 174–179, (1985).

30. Kant R, Llauró A, Rayaprolu V, Qazi S, de Pablo PJ, Douglas T, et al. Changes in the stability and biomechanics of P22 bacteriophage capsid during maturation. Biochimica et Biophysica Acta (BBA) - General Subjects.1862(6):1492-504, (2018).

31. Earnshaw, W. C., and S. R. Casjens. DNA packaging by the double-stranded DNA bacteriophages. Cell. 21:319–331, (1980).

32. Kellenberger, E. Form determination of the heads of bacteriophages. Eur. J. Biochem. 190:233–248, (1990).

33. Thuman-Commike PA, Greene B, Malinski JA, King J, Chiu W. Role of the scaffolding protein in P22 procapsid size determination suggested by T = 4 and T = 7 procapsid structures. Biophys J. 74:559-68, (1998).

34. Parent, K.N., et al., P22 coat protein structures reveal a novel mechanism for capsid maturation: stability without auxiliary proteins or chemical crosslinks. Structure. 18(3): p. 390-401, (2010).

35. Shen W, Yun S, Tam B, Dalal K, Pio FF. Target selection of soluble protein complexes for structural proteomics studies. Proteome Sci. 3(1):3-, (2005).

36. Servid A, Jordan P, O'Neil A, Prevelige P, Douglas T. Location of the Bacteriophage P22 Coat Protein C-Terminus Provides Opportunities for the Design of Capsid-Based Materials. Biomacromolecules. 14(9):2989-95, (2013).

37. Servid AE. Characterization and embellishment of protein cages for nanomedical and nanomaterial applications. (2014).

38. Chen DHB, M. L.; Hryc, C. F.; DiMaio, F.; Jakana, J.; Wu, W. M.; Dougherty, M.; Haase-Pettingell, C.; Schmid, M. F.; Jiang, W.; Baker, D.; King, J. A.; Chiu, W. Proc. Natl. Acad. Sci. U.S.A. 108, 1355−1360, (2011).

39. Kang, S., Lander, G. C., Johnson, J. E., and Prevelige, P. E. Development of bacteriophage P22 as a platform for molecular display: genetic and chemical. (2008).

40. Chen DHB, M. L.; Hryc, C. F.; DiMaio, F.; Jakana, J.; Wu, W. M.; Dougherty, M.; Haase-Pettingell, C.; Schmid, M. F.; Jiang, W.; Baker, D.; King, J. A.; Chiu, W. Proc. Natl. Acad. Sci. U.S.A. 108, 1355−1360, (2011).

41. M. Shah, P. Y. Hsueh, G. Sun, H. Y. Chang, S. M. Janib, J. A. MacKay, Protein Sci. 21, 743, (2012).

42. D. W. Urry, T. M. Parker, M. C. Reid, D. C. Gowda, J. Bioactive Compatible Polym. 6, 263, (1991).

43. Meyer DE, Chilkoti A. Purification of recombinant proteins by fusion with thermally-responsive polypeptides. Nature Biotechnology.17:1112-5, (1999).

44. MacEwan SR, Chilkoti A. Controlled Apoptosis by a Thermally Toggled Nanoscale Amplifier of Cellular Uptake. Nano Letters.14(4):2058-64, (2014).

45. W. Kim, C. Brady, E. L. Chaikof, Acta Biomater. 8, 2476, (2012).

46. A, Rubinstein M. Elastin-like Polypeptide Diblock Copolymers Self-Assemble into Weak Micelles. Macromolecules. 48(12):4183-95, (2015).

47. Lee TAT, Cooper A, Apkarian RP, Conticello VP. Thermo-Reversible Self-Assembly of Nanoparticles Derived from Elastin-Mimetic Polypeptides. Advanced Materials.12(15):1105-10, (2000).

48. Zhang W, Song Y, Eldi P, Guo X, Hayball JD, Garg S, et al. Targeting prostate cancer cells with hybrid elastin-like polypeptide/liposome nanoparticles. Int J Nanomedicine. 13:293-305, (2018).

49. Ghoorchian, A., Cole, J.T., & Holland, N.B. Thermoreversible Micelle Formation Using a Three-Armed Star Elastin-like Polypeptide. Macromolecules, 43, 4340-4345, (2010).

50. Ghoorchian, Ali, et al. "Size and shape characterization of thermoreversible micelles of three-armed star elastin-like polypeptides." The Journal of Physical Chemistry B 117.29 : 8865-8874, (2013).

51. Bettina Kracke, James T. Cole, Christoph J. O. Kaiser, Björn Hellenkamp, Stefanie Krysiak, Ali Ghoorchian, Gary B. Braun, Nolan B. Holland, and Thorsten Hugel Macromolecules 48 (16), 5868-5877, (2015)

52. Cole, James T., "The Synthesis and Characterization of Multifunctional Nanoparticles of Elastin-Like Polypeptides for Theranostic Applications". ETD Archive. 875, (2016).

53. Nath N, Chilkoti A. Interfacial phase transition of an environmentally responsive elastin biopolymer adsorbed on functionalized gold nanoparticles studied by colloidal surface plasmon resonance. J. Am. Chem. Soc.123:8197–8202, (2001).

54. Nath N, Chilkoti A. Creating "smart" surfaces using stimuli responsive polymers. Adv. Mater.14:1243–1247, (2002).

55. Shen W, Yun S, Tam B, Dalal K, Pio FF. Target selection of soluble protein complexes for structural proteomics studies. Proteome Sci. 3(1):3-, (2005).

56. Finkelstein J, Antony E, Hingorani MM, O'Donnell M. Overproduction and analysis of eukaryotic multiprotein complexes in Escherichia coli using a dual-vector strategy. Analytical Biochemistry. 319(1):78-87, (2003).

57. Kerrigan J, Xie Q, Ames R, Lu Q. Production of protein complexes via co-expression. Protein expression and purification. 75:1-14, (2011).

58. Parker, M. H.; Casjens, S.; Prevelige, P. E. J. Mol. Biol. 281, 69−79, (1998).

59. https://www.thermofisher.com/us/en/home/life-science/cloning/cloning-learning-center/invitrogen-school-of-molecularbiology/molecularcloning/transformation/bacterial-transformation-workflow.html

60. https://www.qiagen.com/us/resources/resourcedetail?id=56b0162c-23b0-473c-9229-12e8b5c8d590&lang=en.

61. https://www.thermofisher.com/order/catalog/product/Q32854#/Q32854.

62. https://www.promega.com/products/nucleic-acid-extraction/plasmid-purification/pureyield-plasmid-midiprep-system/?catNum=A2492.

63. Ghoorchian A. Modification of Behavior of Elastin-like Polypeptides by Changing Molecular Architecture: Cleveland State University; (2012).

64. J. K. Deyling, Design and Production of a Hydrogel Forming Polypeptide: Engaging High School Students in Protein Design, Cleveland: Cleveland State University, (2016).

65. http://wolfson.huji.ac.il/expression/procedures/bacterial/AutoInduced-Media.pdf.

66. Pace CN, Vajdos F, Fee L, Grimsley G, Gray T. How to measure and predict the molar absorption coefficient of a protein. Protein Sci. 4(11):2411-23, (1995).

67. Correa A, Oppezzo P. Tuning different expression parameters to achieve soluble recombinant proteins in E. coli: Advantages of high-throughput screening. Biotechnology Journal. 6(6):715-30, (2011).

68. Correa A, Oppezzo P. Overcoming the solubility problem in E. coli: available approaches for recombinant protein production. Insoluble proteins: Springer; p. 27-44, (2015).

69. Meyer DE, Chilkoti A. Quantification of the Effects of Chain Length and Concentration on the Thermal Behavior of Elastin-like Polypeptides. Biomacromolecules. 5(3):846-51, (2004).

70. Ghoorchian A, Holland NB. Molecular Architecture Influences the Thermally Induced Aggregation Behavior of Elastin-like Polypeptides. Biomacromolecules. 12(11):4022-9, (2011).

71. Botstein D, Waddell CH, King J. Mechanism of head assembly and DNA encapsulation in Salmonella phage P22: I. Genes, proteins, structures and DNA maturation. Journal of Molecular Biology. 80(4):669-95, (1973).

72. McPherson DT, Xu J, Urry DW. Product Purification by Reversible Phase Transition Following Escherichia coli Expression of Genes Encoding up to 251

Repeats of the Elastomeric Pentapeptide GVGVP. Protein Expression and Purification. 7(1):51-7, (1996).

73. Schwarz B. Biomimetic structural engineering of P22 virus-like particles for catalysis and immune modulation, (2016).

74. MacEwan SR, Chilkoti A. Applications of elastin-like polypeptides in drug delivery. Journal of Controlled Release. 190:314-30, (2014).

75. Murtey MD, Ramasamy P. Sample Preparations for Scanning Electron Microscopy – Life Sciences. Modern Electron Microscopy in Physical and Life Sciences, (2016).

76. Smits FC, Buddingh BC, van Eldijk MB, van Hest JC. Elastin-like polypeptide-based nanoparticles: design rationale toward nanomedicine. Macromol Biosci. 15(1):36-51, (2015).

77. Deyling JK, Turk EM, Holland NB. Preparing Genes for Repetitive Elastin-Like Polypeptides Using Gibson Assembly. Methods Mol Biol. 1798:265-275, (2018).

78. Dynamic Light Scattering: An Introduction in 30 Minutes, Technical Note, Malvern Instrument Limited, (2017).

Appendix A

Auto-Induction Media:

1. 10 g of tryptone, 5 g yeast extract, 3.3 g ammonium sulfate (25 mM), 6.8 g monopotassium phosphate (50 mM), 7.1 g disodium phosphate (50 mM), and 0.15 g magnesium sulfate (1.25 mM) are added to 1 L of deionized water and mixed up thoroughly.
2. The Erlenmeyer flask containing the ingredients was autoclaved for an hour at 120℃.
3. In another small container 0.5 g glucose and 2g α-lactose was dissolved thoroughly and was filtered using 220 µm disk-filter.
4. Once the content of Erlenmeyer flask (1 L solution) reached less than 40°C the sugar solution (from step 3) and 0.1 g ampicillin were added to make the final auto-induction broth.

Auto-Induction Expression Protocol:

1. The contents of two 5 mL overnight cultures were poured into 1 L of prepared auto-induction media.
2. The batch containing bacteria of interest was inserted into an incubator shaker for 30 h of incubation at 25°C with the speed of 200 RPM (as a rule of thumb for 2°C decrease in temperature would add 1 h of incubation). Enough holes were poked on the aluminum foil cap to assure the content are well-aerated during that long time.

3. The whole batch was poured into a 1 L centrifuge jar and balanced with another 1 L jar in the centrifuge for a 45 min cycle of 4200 RPM.
4. The supernatant was discarded and cell pellets were collected in the 1 L centrifuge container.
5. The centrifuge jar was saved in the freezer (at -20°C) for the purification step.

Appendix B

Purification Protocol (for CP-H10 and CP-H40 Constructs):

1. The bacterial pellet (~15-20 g) was resuspended in 35 mL of PBS (in a Falcon 50 mL) and vortexed for a well-mixed solution.
2. Cell resuspension was lysed using pulse sonication at the power level of 7 for 9 runs of 10s on/ 30s off.
3. Put the sample on ice for 10-15 min (to cool down the lysate) then run the 1st cold cycle at 15℃ for 30 min of 10000 RPM.
4. The supernatant (brownish color) were collected and transferred to a new 50 mL centrifuge tube. Both solutions were placed into the incubator at 60℃ a period of 30 min for the phase separation (coacervate) to happen.
5. Since phase separation was not complete for CP-H10 ammonium sulfate was added to a final concentration of 1 M (~5 g). During this stage the brownish (clear) color of solution turn int milky (cloudy/ turbid). No ammonium sulfate needed CP-H40 as phase separation was complete.
6. Run the 1st hot cycle centrifugation at 11000 RPM and 15 min at 40℃ to precipitate the protein of interest.
7. Discard the supernatants for both solutions and resuspend the obtained hot-pellet in 15 mL PBS (the solution ratio always could be adjusted base on the pellet mass). Break the pellet and mix thoroughly (i.e. using glass-beads).

8. Let sample cool down in the fridge for 10 min, right after centrifuge for the 2nd cold cycle at 15°C for 30 min of 10000 RPM.
9. Collect the supernatant and put it in the incubator for 30 min at 60°C right before running the 2nd hot cycle.
10. Run the 2nd hot cycle centrifugation at 11000 RPM and 15 min at 40°C to precipitate the protein. The supernatants were discarded and pellets were collected for future analysis.
11. (OPTIONAL) You might run another extra cold cycle (3rd) to make the sample more purified

Appendix C

SEM Instrumentation:

The SEM instrument in use for this study was FEI-Quanta Nova-SEM (physics department, Cleveland State University).

1. After sample preparation using the "Vent" button (to do the sample chamber's evacuation) sample was mounted on the grounded XYZ stage.
2. Samples are attached on the top of the standardized stub (make sure there is no possibility for sample's detachment) which could be fitted with this stage and be tightened using a set screw. This stage is manually adjustable for height level, rotation, and tilt of the sample (a standard sample holder has a diameter of 10 mm)
3. Controlling the Z-distance is done using stage knob which is located on the outside of the chamber door. As a rule of thumb, the sample should be able to clear the bottom of the column by at least 10 mm.
4. Close the chamber's door and click on the "Pump" button.
5. After reaching the vacuum threshold the chamber's icon turning the color into the green, which means the instrument is ready for the beam emission.
6. The acceleration voltage is set to 5-10 kV for a more observable picture as well as a less deleterious condition for the specimen. Other parameters including magnification, focus, and brightness/ contrast were regulated manually.